

AD-A042 192

UNIVERSAL ENERGY SYSTEMS INC DAYTON OHIO

F/G 20/8

STUDIES OF THE FACTORS AFFECTING THE ANALYSIS OF THIN FILMS AND--ETC(U)

MAY 77 J T GRANT

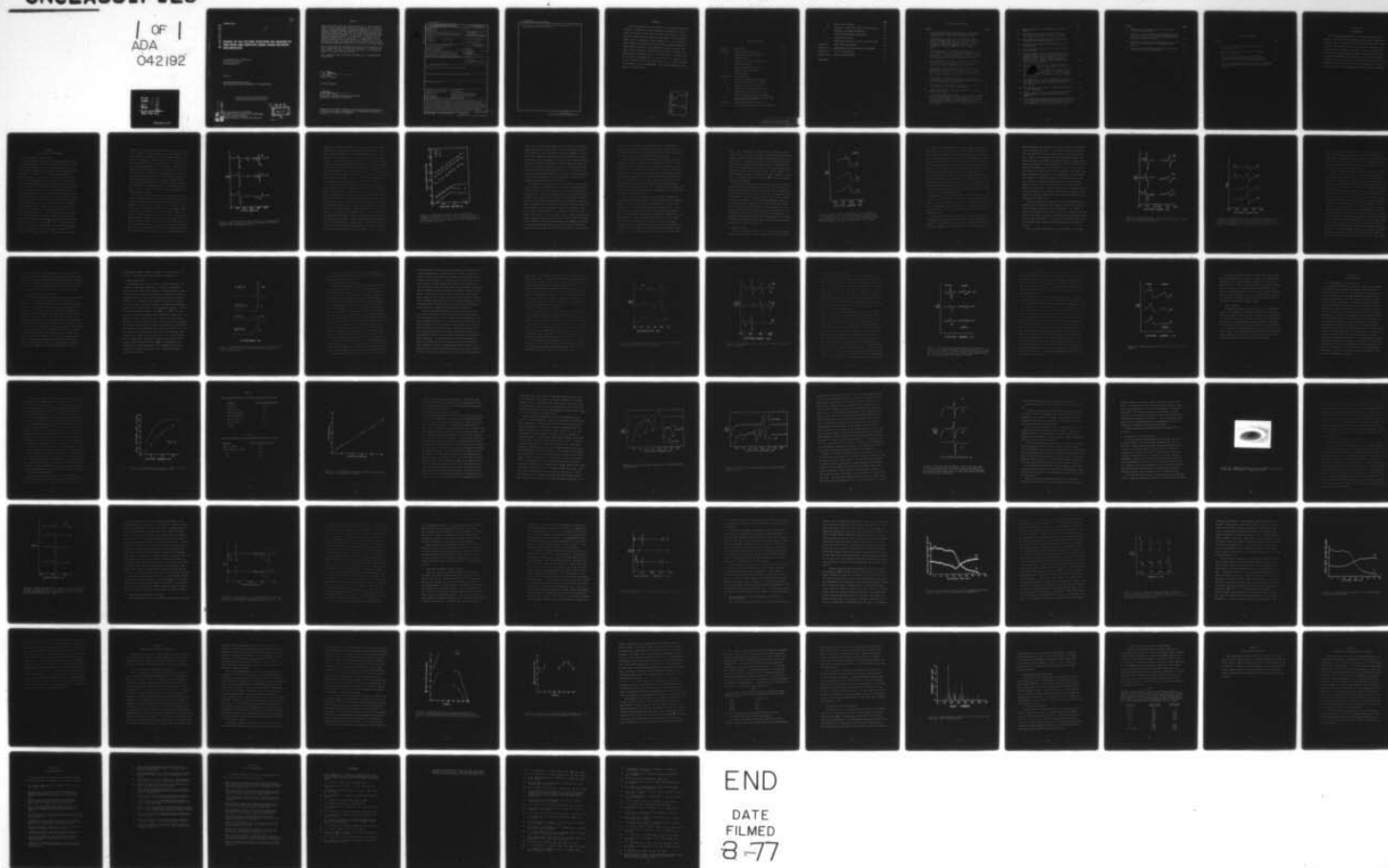
F33615-74-C-4017

UNCLASSIFIED

AFML-TR-77-52

NL

1 OF 1
ADA
042192



END

DATE
FILMED
8-77

AD A 042192

AFML-TR-77-52

12

**STUDIES OF THE FACTORS AFFECTING THE ANALYSIS OF
THIN FILMS AND SURFACES USING AUGER ELECTRON
SPECTROSCOPY**

*UNIVERSAL ENERGY SYSTEMS, INC.
3195 PLAINFIELD ROAD
DAYTON, OHIO 45432*

MAY 1977

TECHNICAL REPORT AFML-TR-77-52
FINAL REPORT FOR PERIOD DECEMBER 1973 - DECEMBER 1976

Approved for public release; distribution unlimited

AD No. _____
DDC FILE COPY

AIR FORCE MATERIALS LABORATORY
AIR FORCE WRIGHT AERONAUTICAL LABORATORIES
AIR FORCE SYSTEMS COMMAND
WRIGHT-PATTERSON AIR FORCE BASE, OHIO 45433

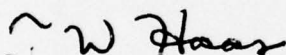
DDC
JUL 27 1977
D

NOTICE

When Government drawings, specifications, or other data are used for any purpose other than in connection with a definitely related Government procurement operation, the United States Government thereby incurs no responsibility nor any obligation whatsoever; and the fact that the Government may have formulated, furnished, or in any way supplied the said drawings, specifications, or other data, is not to be regarded by implication or otherwise as in any manner licensing the holder or any other person or corporation, or conveying any rights or permission to manufacture, use, or sell any patented invention that may be related in any way thereto.

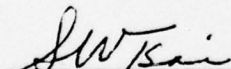
This report has been reviewed by the Information Office (OI) and is releasable to the National Technical Information Service (NTIS). At NTIS, it will be available to the general public, including foreign nations.

This technical report has been reviewed and is approved for publication.



T. W. Haas
Project Engineer

FOR THE DIRECTOR



S. W. Tsai, Chief
Mechanics & Surface Interactions Branch
Nonmetallic Materials Division

Copies of this report should not be returned unless return is required by security considerations, contractual obligations, or notice on a specific document.

UNCLASSIFIED

SECURITY CLASSIFICATION OF THIS PAGE (When Data Entered)

17 REPORT DOCUMENTATION PAGE		READ INSTRUCTIONS BEFORE COMPLETING FORM
1. REPORT NUMBER AFML-TR-77-52	2. GOVT ACCESSION NO.	3. RECIPIENT'S CATALOG NUMBER
4. TITLE (and Subtitle) STUDIES OF THE FACTORS AFFECTING THE ANALYSIS OF THIN FILMS AND SURFACES USING AUGER ELECTRON SPECTROSCOPY.	5. TYPE OF REPORT & PERIOD COVERED Final Report 17 Dec 73 - 17 Dec 76	
7. AUTHOR(s) J. T. Grant	8. CONTRACT OR GRANT NUMBER(s) F33615-74-C-4017	
9. PERFORMING ORGANIZATION NAME AND ADDRESS Universal Energy Systems, Inc. 3195 Plainfield Road Dayton, Ohio 45432	11. PROGRAM ELEMENT, PROJECT, TASK AREA & WORK UNIT NUMBERS 23030102	
11. CONTROLLING OFFICE NAME AND ADDRESS Air Force Materials Laboratory (AFML/MBM) Air Force Wright Aeronautical Laboratories Wright-Patterson Air Force Base, Ohio 45433	12. REPORT DATE May 1977	
14. MONITORING AGENCY NAME & ADDRESS (if different from Controlling Office)	13. NUMBER OF PAGES 88	
	15. SECURITY CLASS. (of this report) Unclassified	
16. DISTRIBUTION STATEMENT (of this Report) Approved for public release; distribution unlimited		
17. DISTRIBUTION STATEMENT (of the abstract entered in Block 20, if different from Report)		
18. SUPPLEMENTARY NOTES		
19. KEY WORDS (Continue on reverse side if necessary and identify by block number) Auger Electron Spectroscopy Ion Bombardment Surface Analysis Appearance Potential Spectroscopy Thin Films X-Ray Photoelectron Spectroscopy Depth Profiling Secondary Ion Mass Spectroscopy Surface Physics Surface Chemistry		
20. ABSTRACT (Continue on reverse side if necessary and identify by block number) This report describes the results of a research program undertaken to study the factors affecting the analysis of thin films and surfaces using Auger electron spectroscopy. Problems in interpreting Auger data both qualitatively and quantitatively due to overlap of spectral lines, chemical shifts in spectra, changes in spectral line shape, electron beam interactions and sample charging have been investigated and methods to overcome them have been developed. Problems that arise in depth profiling solids by inert gas ion bombardment → next page		

DD FORM 1 JAN 73 1473 EDITION OF 1 NOV 65 IS OBSOLETE

UNCLASSIFIED

SECURITY CLASSIFICATION OF THIS PAGE (When Data Entered)

390 743

UNCLASSIFIED

SECURITY CLASSIFICATION OF THIS PAGE(When Data Entered)

→ have also been studied and techniques to improve the reliability of such measurements have also been developed. ↗

UNCLASSIFIED

SECURITY CLASSIFICATION OF THIS PAGE(When Data Entered)

FOREWORD

This report describes the results of a research program undertaken to study the factors affecting the analysis of thin films and surfaces using Auger electron spectroscopy. The program was conducted during the period December 1973 through December 1976 by Universal Energy Systems, Inc., 3195 Plainfield Road, Dayton, Ohio 45432, at the Air Force Aerospace Research Laboratories and the Air Force Materials Laboratory under Contract F33615-74-C-4017, initiated under Task No. 2303Q1. The research was performed by Dr. J. T. Grant and M. P. Hooker with the technical assistance of R. G. Wolfe and J. R. Miller. The Project Engineer for the Air Force was Dr. T. W. Haas, Nonmetallic Materials Division (AFML/MBM). The authors submitted this report in February 1977.

ACCESSION for		
NTIS	White Section	<input checked="checked" type="checkbox"/>
DDC	Buff Section	<input type="checkbox"/>
UNANNOUNCED		<input type="checkbox"/>
JUSTIFICATION		
BY		
DISTRIBUTION/AVAILABILITY CODES		
Dist.	Avail.	and/or SPECIAL
A		

TABLE OF CONTENTS

	<u>Page</u>
SECTION I. INTRODUCTION	1
SECTION II. AUGER ELECTRON SPECTROSCOPY	2
A POTENTIAL MODULATION DISTORTION	2
B CHEMICAL EFFECTS	9
C EFFECTS DUE TO ELECTRON ENERGY LOSS	16
D SAMPLE POSITIONING	17
E SPECTRUM SUBTRACTION TECHNIQUES	19
F ELECTRON BEAM INTERACTIONS	24
G SAMPLE CHARGING	28
SECTION III. DEPTH PROFILING	29
A ION GUN SPUTTERING RATE CALIBRATION	29
B ION EXCITED AUGER ELECTRON SPECTRA	34
1. Application to ion gun alignment	41
2. Interference during depth profiling	43
C ELECTROSTATIC SHIELDING OF ION GUNS	45
D SOME OTHER PROBLEMS IN DEPTH PROFILING	48
E THE APPLICATION OF TAILORED MODULATION TECHNIQUES TO DEPTH PROFILING	51
SECTION IV. OTHER SURFACE ANALYSIS TECHNIQUES	59
A SOFT X-RAY APPEARANCE POTENTIAL SPECTROSCOPY	59

	<u>Page</u>
1. Quantitative aspects	60
2. Comparison with Auger electron spectroscopy	65
B SECONDARY ION MASS SPECTROSCOPY	66
C X-RAY PHOTOELECTRON SPECTROSCOPY	68
1. Standard XPS spectra	68
2. Comparison with Auger electron spectroscopy	69
SECTION V. DEPTH PROFILE ANALYSES	70
SECTION VI. CONSTRUCTION AND MAINTENANCE OF EQUIPMENT	71
SECTION VII. LIST OF PUBLICATIONS	72
SECTION VIII. LIST OF PRESENTATIONS	74
REFERENCES	76

LIST OF ILLUSTRATIONS

<u>Figure</u>	<u>Page</u>
1. First derivative Auger spectra of a contaminated nickel surface taken using different modulation amplitudes (a) 1 eV, (b) 5 eV and (c) 25 eV.	4
2. Dependences of Auger signal strengths on modulation amplitude measured (i) from peak-to-peak heights in $\mathcal{N}_m^{(1)}(E)$, curves A, B, and C and (ii) as Auger area values obtained by double integration of appropriate $\mathcal{N}_m^{(1)}(E)$ data, curves D, E, and F.	6
3. First integrals of derivative Auger spectra of C on Ni(110) : (a) following exposure of clean Ni(110) to 1×10^{-4} Pa of CO for 15 min; (b) after exposure to the electron beam for 10 min; (c) after exposure to the electron beam for 40 min.	10
4. Auger spectra of C (left hand side) and O (right hand side) following exposure of CO to clean surfaces of Nb(top), Co(middle) and Pt(bottom).	13
5. First derivative oxygen KVV Auger spectra for room temperature oxygen exposures to Ni (110) at (a) 8×10^{-4} , (b) 2.4×10^{-3} , (c) 4.0×10^{-3} , and (d) 9.6×10^{-3} Pa.s. Parts (a) and (b) are shown magnified 2X relative to parts (c) and (d).	14
6. Illustration of the application of integration techniques to correct for small sample misalignment using a retarding field analyzer.	18
7. Illustration of the application of SST to enhance the detection of sulfur on molybdenum.	22
8. Illustration of the application of SST to retrieve Auger line shapes.	23
9. First derivative Auger spectra of C and O on Ni(110): (a) following exposure of clean Ni(110) to 1×10^{-4} Pa of CO for 15 min; (b) after exposure to the electron beam for 10 min; (c) after exposure to the electron beam for 40 min. The electron beam was $1.5 \mu A$ at 1.5 keV.	25

	<u>Page</u>
10. First integrals of the respective data shown in Figure 9.	27
11. Sputtering rate calibration curves for Ta ₂ O ₅ films using model 04-161 and 04-191 ion guns.	31
12. Time required to sputter through Ta ₂ O ₅ films as a function of anodization voltage.	33
13. Low energy Auger spectrum of Al excited by 2keV electron beam.	36
14. Low energy Auger spectrum of Al excited by 3keV argon ion beam.	37
15. Electron excited (part a) and ion-excited (part b) Auger spectra of main Al features taken under identical experimental conditions. Part (c) shows the result obtained after subtracting a fraction of the electron excited spectrum from the ion excited spectrum.	39
16. Example of precise ion gun alignment using ion excited Auger spectroscopy. Magnification 20X.	42
17. LMM Auger spectra of Mg taken (a) with a 10μA, 2000 eV ion beam, (b) with a 6 μA, 3000 eV electron beam, and (c) with these two beams on simultaneously. Part (d) is the sum of the data shown in (a) and (b).	44
18. Auger spectra of a flashed stainless steel specimen taken (a) with the ion bombardment gun off and (b) with the high voltage (2000 V) applied to the ion gun.	46
19. Illustration of the effect of sample charging due to ion bombardment.	50
20. Depth profile of Al ₂ O ₃ on Al obtained using peak-to-peak heights in first derivative spectra $N_m^{(1)}(E)$.	53
21. First derivative AlKL _{2,3} L _{2,3} Auger spectra from Al ₂ O ₃ on Al after sputtering for various times: (a) before sputtering; (b) 5 min; (c) 20 min; (d) 30 min; (e) 33 min; (f) 37 min; (g) 40 min; (h) 65 min.	55

<u>Figure</u>	<u>Page</u>
22. Depth profile of Al_2O_3 on Al using Auger area values obtained with TMT.	57
23. Relative L_3 and L_2 APS signal strengths of Ti, V, Fe, Co, Ni ³ and Cu ² measured as the peak-to-peak deflections of their first derivative spectra. No peaks were detected from Cu.	62
24. Combined L_3 , L_2 APS signal strengths from Ti, V, Fe, Co, Ni and ³ Cu measured using integration techniques.	63
25. SIMS spectrum of negative ions emitted by Al surface under argon ion bombardment.	67

LIST OF TABLES

<u>Table</u>	<u>Page</u>
1. Argon sputtering rates for some materials relatives to Ta ₂ O ₅ .	32
2. Xenon sputtering rates for some materials relative to Ta ₂ O ₅ .	32
3. L ₃ /L ₂ APS signal strength ratios for some 3d metals obtained from peak-to-peak height measurements in first derivative APS spectra.	65
4. Ratios of corresponding Ni XPS or X-ray excited AES signal strengths obtained from heavily oxidized Ni to clean Ni.	69

SECTION I
INTRODUCTION

The elemental composition of the few outermost atomic layers of a solid can be determined using Auger electron spectroscopy (AES). Problems in interpreting AES data both qualitatively and quantitatively due to overlap of spectral lines, chemical shifts in spectra, changes in spectral line shape, electron beam interactions and sample charging have been investigated and methods to overcome them have been developed. Problems that arise in depth profiling solids by inert gas ion bombardment have also been studied and techniques to improve the reliability of such measurements have also been developed.

SECTION II

AUGER ELECTRON SPECTROSCOPY

A. Potential Modulation Distortion

The most common method for producing Auger electrons is by electron beam impact. In the case of gaseous targets the Auger electron energy distribution can be measured directly and the relative Auger currents can be obtained from the measured Auger intensities. In contrast, for solid targets the number of Auger electrons in a given energy range is small relative to the number of background electrons that are due to the production of secondary and backscattered electrons from the target, so Auger electron currents cannot be measured directly from such electron energy distributions. This background electron current varies with the energy measured and must be removed to obtain a measure of the Auger currents. There have been a number of approaches made to achieve this, the most common of which is to differentiate the electron energy distribution to suppress the more slowly varying background, and use the peak-to-peak heights of the enhanced, derivative Auger features as a measure of the Auger currents.¹ The first derivative of the electron energy distribution is usually sufficient to remove or satisfactorily reduce the background, the distribution then obtained being referred to here as $\mathcal{N}_m^{(1)}(E)$. Derivative Auger spectra can be obtained directly by using potential modulation (sinusoidal) and phase sensitive detection techniques^{2,3} and form a basis for quantitative Auger analysis by comparing mea-

sured first derivative spectra with appropriate standard spectra.¹ However, to obtain accurate comparative values for Auger currents the line shapes of the measured and standard spectra have to be identical. Although this is often the case, situations arise where this is not possible, e.g., where changes in the chemical environment of an element under study produce changes in the Auger electron energy distribution⁴ (see subsection B below). Further, the detectability of a given element can generally be improved by increasing the sinusoidal modulation amplitude, but above a certain modulation amplitude the peak-to-peak height of a particular Auger feature does not increase in a well-defined manner with modulation amplitude (in fact, it also can decrease) making quantitative measurements less reliable.

The effects of potential modulation distortion have been analyzed, assuming a Gaussian Auger peak shape, for both types of energy analyzers commonly used in Auger electron spectroscopy^{5,6}. In the case of a deflection type analyzer, it was found that the first-harmonic signal strength increased linearly with modulation amplitude up to an amplitude of about $0.3p$, where p is the Gaussian root mean square width. The signal then passed through a maximum and subsequently decreased at a rate near the inverse square root of the modulation amplitude for values in excess of about $3p$. For a retarding field type analyzer, where the second harmonic is detected in order to obtain the first derivative of the electron energy distribution, the

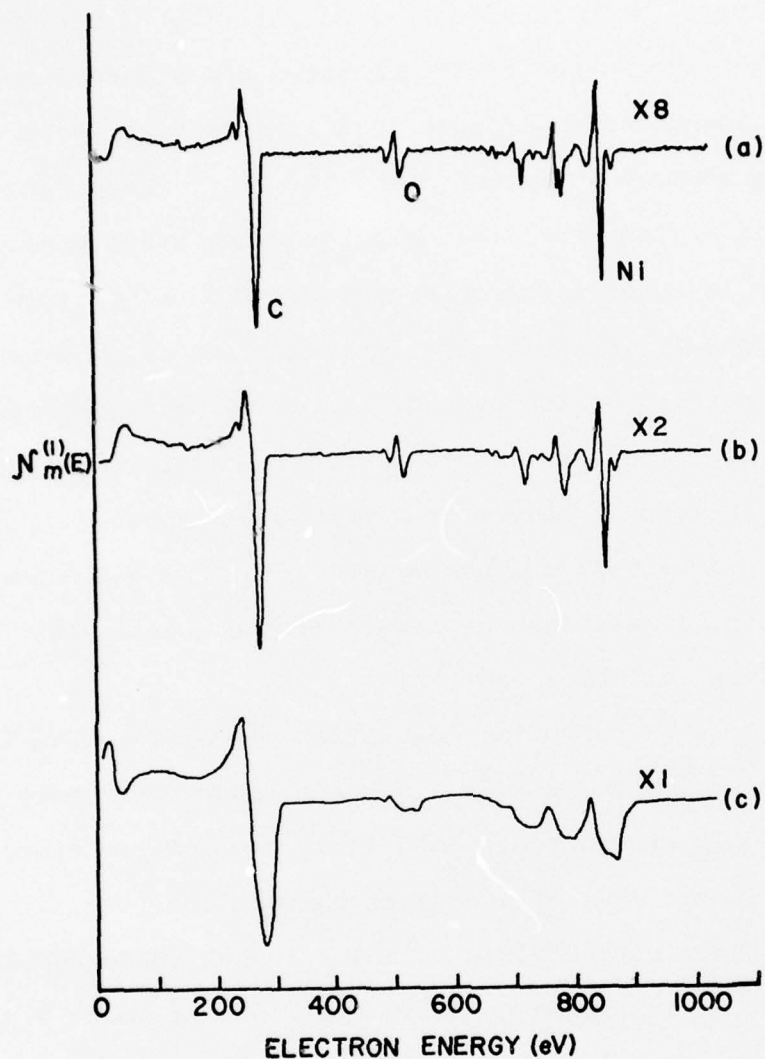


Figure 1 - First derivative Auger spectra of a contaminated nickel surface taken using different modulation amplitudes (a) 1 eV, (b) 5 eV and (c) 25 eV.

signal was found to increase as the square of the modulation amplitude up to about 0.5p after which it approaches a constant value independent of the modulation amplitude. The behavior of the derivative Auger signal as the modulation amplitude is increased depends on the detailed shape of the Auger feature in the electron energy distribution. The calculations just mentioned were based on a Taylor series formalism and are strictly valid only for a Gaussian peak shape. Furthermore, the Taylor series method of analysis is an approximate one and has little utility except in the region where the modulation amplitudes are small with respect to the feature widths.

The effects of (sinusoidal) modulation amplitude on first derivative C, O and Ni Auger spectra taken using a cylindrical mirror analyzer ($\Delta E/E \approx 0.005$) are shown in Figure 1. These spectra were taken under identical experimental conditions except that the modulation amplitude used was different for all three. Figure 1(a) is essentially a high resolution spectrum (modulation amplitude 1 eV) showing the presence of carbon and oxygen at the nickel surface, and the carbon line shape indicates it to be present in graphitic form⁴. For this spectrum the modulation amplitude is sufficiently small compared with the widths of the carbon, oxygen, and nickel Auger features so as not to add distortion to their shapes. For such high resolution spectra the peak-to-peak heights of the Auger features increase linearly with modulation amplitude. Figure 1(b) was

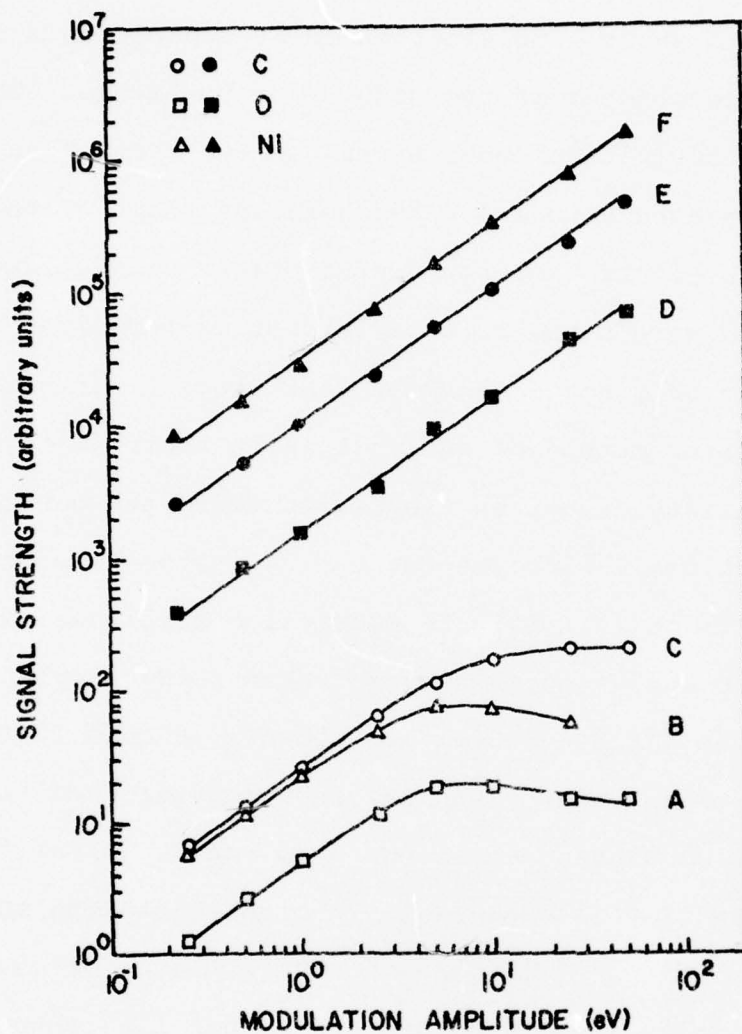


Figure 2 - Dependences of Auger signal strengths on modulation amplitude measured (i) from peak-to-peak heights in $\mathcal{N}_m^{(1)}$ (E), curves A, B, and C and (ii) as Auger area values obtained by double integration of appropriate $\mathcal{N}_m^{(1)}$ (E) data, curves D, E, and F.

taken with a modulation amplitude of 5 eV, and it can be seen that although all the main Auger features have bigger peak-to-peak values they have increased by different amounts. This is because the modulation amplitude is now comparable with Auger peak widths and the changes in signal size with modulation will depend on the Auger peak shapes. With a modulation amplitude of 25 eV the carbon feature is bigger yet, but the oxygen and nickel features have decreased, Figure 1(c). Of course, the use of large modulation amplitudes to improve sensitivity broadens the Auger features and often precludes any chemical information being obtained from such data.

The dependences of the peak-to-peak heights of the largest carbon, oxygen, and nickel Auger features on modulation amplitude are shown in Figure 2, curves C, A, and B, respectively. It can be seen that for amplitudes below 1 eV, the peak-to-peak heights scale together and linearly with modulation, whereas above 1 eV the peak-to-peak heights vary differently, making accurate measurements of relative Auger currents of different elements directly from such spectra virtually impossible. However, having complete data as a function of modulation amplitude as in curves A, B, and C would allow accurate comparisons of Auger currents to be made from first derivative Auger data when either different surface concentrations are present or when different modulation amplitudes are used, so long as line shape changes due to chemical effects are not involved. Curves such

as these are not generally available and it is difficult to compare, for example, the relative concentrations of a particular contaminant on different nickel surfaces taken using similar analyzers under different effective resolutions.

However, using an instrument response formalism it has recently been shown that under the assumptions (1) that the background has been eliminated in the spectrum in derivative form and (2) that the Auger signal consists of a peak in the energy distribution, then the area under the Auger feature determined by the double integral of the measured derivative spectrum over the entire structure can be simply and exactly related to the area measured in the absence of potential modulation distortion^{7,8}. It was further shown that this simple relationship did not depend on the detailed shape of the Auger peak and was valid for all modulation amplitudes.

The results for a cylindrical mirror analyzer obtained by doubly integrating the carbon, oxygen, and nickel data shown in Figure 1 are plotted in Figure 2 and labeled E, D, and F, respectively. It can be seen that Auger area values Y_t , for carbon, oxygen, and nickel, measured as these double integrals, have an exact, linear dependence on modulation amplitude e_0 , for amplitudes up to 50 eV, the experimental limit in this work. By defining the measured Auger currents I_A , by $I_A = Y_t/e_0$, current values are obtained for carbon, oxygen, and nickel, independent of the modulation amplitude used and could be readily compared with corresponding Auger currents from suitable stan-

dards. The corresponding relationship for a retarding field analyzer⁹ is $I_A = Y_t/e_0^2$. Integration has been carried out using analog and digital techniques, both techniques being quite successful.^{10,11} Problems in comparing Auger data taken with different modulation amplitudes no longer arise. Using such integration techniques makes it feasible to use large modulation amplitudes to obtain better signal-to-noise ratios in $\mathcal{N}_m^{(1)}(E)$ data, thereby improving the sensitivity, while obtaining a value for I_A independent of the distortion in $\mathcal{N}_m^{(1)}(E)$ due to large modulation amplitudes.

The Auger area values obtained depend on the energy range over which the integrations are carried out due to the tails on the low energy sides of the Auger peaks¹⁰ so the low energy integration limit has to be kept constant for the particular Auger transition(s) under study, and the same as that used in obtaining I_A from a standard. Useful comparisons between Auger currents from different elements having simple Auger line shapes can be made from their Auger current values obtained by integrating through the same energy range and then applying any experimental corrections (such as variation of energy window of analyzer with energy) to the data¹⁰. Improvement in the signal-to-noise of Auger data following integration has been noted and details can be read in Reference 9.

B. Chemical Effects

Important information about surface bonding can be obtained from Auger spectra when valence electrons are involved in the

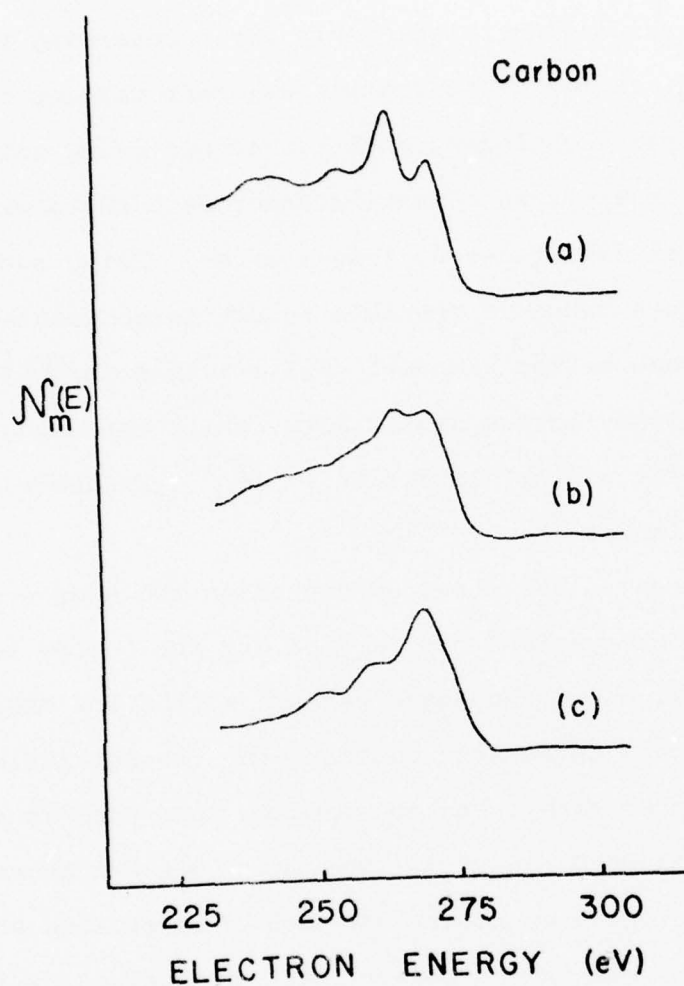


Figure 3 - First integrals of derivative Auger spectra of C on Ni(110) : (a) following exposure of clean Ni(110) to 1×10^{-4} Pa of CO for 15 min; (b) after exposure to the electron beam for 10 min; (c) after exposure to the electron beam for 40 min. The electron beam was $1.5 \mu\text{A}$ at 1.5 keV .

Auger process.⁴ Interpretation is simpler when only one valence electron is involved in the Auger process,¹² as when two valence electrons participate convolution products of density of states functions are involved.¹³ Good correspondence between Auger data and band structure has been found.^{12,13} However, some LVV Auger spectra (of solids) show distinct characteristics of free-atom spectra and do not reflect the band structure, possibly because of electron localization due to increased screening.¹⁴ However, the line shapes of Auger spectra are often useful as a method for fingerprinting the chemical form of surface atoms, e.g. in the case of carbon, to distinguish between graphite-like overlayers and surface carbides on metals and semiconductors, or the different bonding mechanics of CO to clean metal surfaces.

Examples of various carbon Auger line shapes observed from carbon on nickel are shown in Figure 3. These spectra are displayed as Auger electron energy distributions, part(a) being from CO absorbed on clean nickel, and part(b) being from partly decomposed CO on clean nickel, and part(c) being from a nickel carbide surface.

Studies of both the carbon and oxygen Auger line shapes following the absorption of CO on clean transition metal surfaces have been used to characterize the bonding of CO to metal surfaces. Examples of the carbon and oxygen Auger spectra ob-

served following the exposure of clean Nb Co and Pt surfaces to CO are shown in Figure 4. The carbon spectra are shown on the left hand side and the oxygen spectra on the right hand side. Note the differences in Auger line shapes between the carbon spectra, and between the oxygen spectra. (Spectrum subtraction techniques - see subsection E - had to be used to determine the carbon Auger line shape for CO on Pt due to overlap between the carbon and Pt Auger features). The Auger line shapes observed were found to correlate with previous absorption models for transition metals - CO decomposes on Ta, Nb and Ti while it absorbs molecularly on Pd, Ir and Pt where bonding occurs via the carbon atom with its molecular axis normal to the surface. CO was found to partly decompose on Co. Further details as to how these differences in bonding are reflected in both the carbon and oxygen Auger line shapes can be obtained from Reference 15.

Changes in Auger line shape have also been observed and studied for both adsorbate and substrate during the exposure of clean surfaces to gases at room temperature. For example, in studying the absorption of oxygen on nickel, changes in the oxygen KVV and nickel L_3 VV Auger line shapes with increasing oxygen exposure were documented¹⁶. Examples of the oxygen Auger spectra observed after several different exposures are shown in Figure 5.

When only core level electrons are involved in the Auger

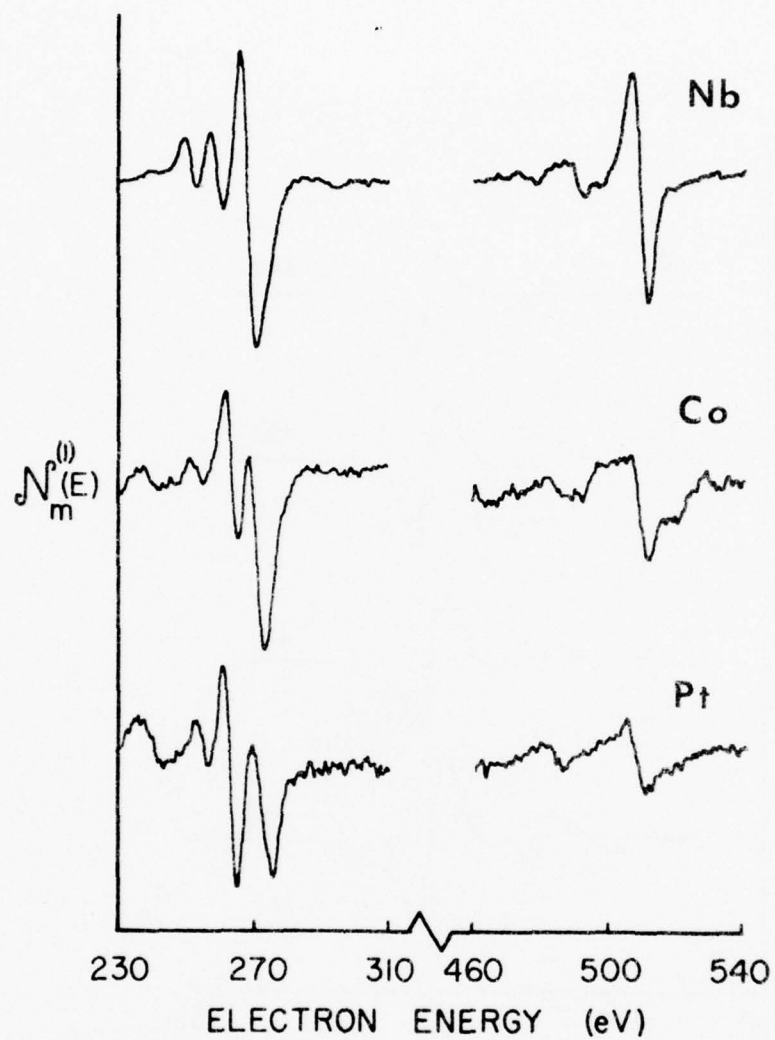


Figure 4 - Auger spectra of C (left hand side) and O (right hand side) following exposure of CO to clean surfaces of Nb (top), Co (middle) and Pt (bottom).

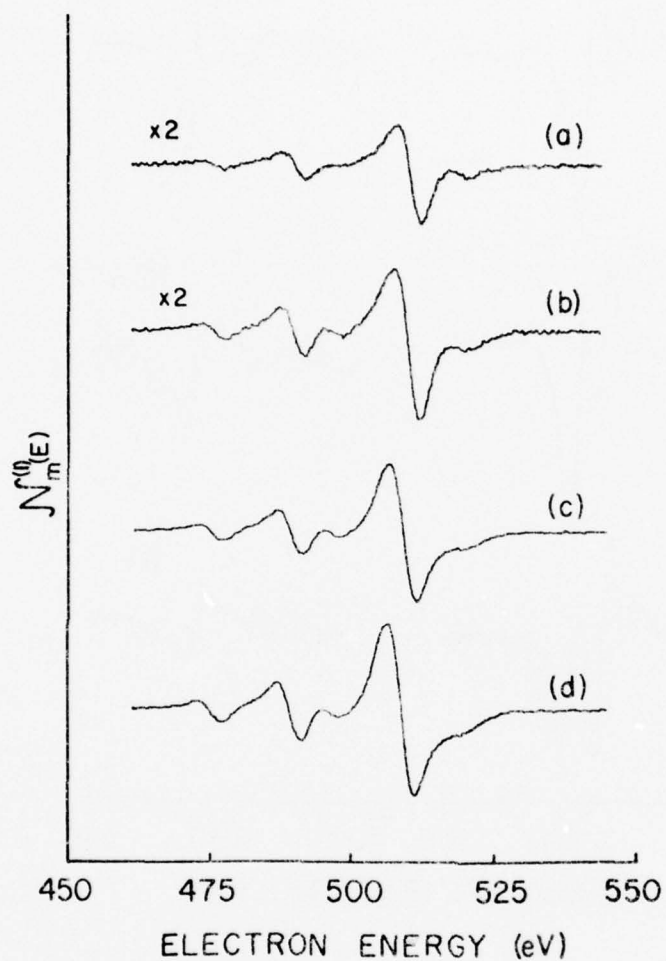


Figure 5 - First-derivative oxygen KVV Auger spectra for room temperature oxygen exposures to Ni (110) at (a) 8×10^{-4} , (b) 2.4×10^{-3} , (c) 4.0×10^{-3} , and (d) 9.6×10^{-3} Pa.s. Parts (a) and (b) are shown magnified 2X relative to parts (c) and (d).

process, changes in bonding may be reflected as a shift in the Auger energy¹⁷ and such measurements may also be useful as an aid to compound identification when large energy shifts (\sim few eV) occur^{18,19}. Shifts in Auger energy are also observed for transitions involving bonding electrons - further details of this work can be read in References 16 and 20.

Although chemical effects in Auger spectroscopy are often quite useful for characterizing the chemical environment of surface atoms they posed a problem in quantitative analysis. If peak-to-peak heights in derivative Auger spectra are used for quantitative analysis the measured line shapes must be identical with those of standards¹. This is not always possible and where changes between observed and standard spectra occur the accuracy of this method decreases, the decrease depending on the degree of line shape changes. This problem in comparing Auger signal strengths has been investigated and solved by doubly integrating first derivative spectra to obtain relative measures of Auger currents. In fact these integration techniques have also been used to compare Auger currents from different elements, having quite different Auger line shapes, on the same surface. Studies of the adsorption of submonolayer amounts of CO absorbed on clean Mo and Ni surfaces showed that the use of carbon and oxygen Auger peak-to-peak heights in first derivative data did not indicate equal numbers of carbon and oxygen atoms were present following adsorption, whereas by doubly integrating the carbon and oxygen Auger features through the same energy range and by comparing these integrated signal strengths it was shown that equal numbers

of carbon and oxygen atoms were present on both surfaces^{10,21}. This result is quite significant because not only are the carbon and oxygen Auger line shapes different from each other, but both the carbon and oxygen line shapes are also different for CO and Mo and Ni due to the different bonding between CO and these two metals. Further details can be read in References 10 and 21.

C. Effects Due to Electron Energy Loss

Even when only core level electrons are involved in an Auger transition its measured line shape can vary with chemical environment due to different energy loss mechanisms that can occur while the Auger electron travels through the lattice before escaping into the vacuum. These different loss mechanisms will affect the electron mean free path for inelastic collisions and therefore the overall electron mean free path. However, the measured Auger signals from such samples can still be compared by using integration techniques, although the relative Auger signal strengths now depend somewhat on the energy range of integration²².

When changes in Auger line shape also occur due to chemical effects useful comparisons between data can still be made using integration techniques. For example in comparing Ni LMM Auger signal strengths between clean and heavily oxidized Ni surfaces relative Auger current measurements based on peak-to-peak heights in $\mathcal{N}_m^{(1)}(E)$ are not self-consistent, whereas

measurements based on double integrals of the data are consistent. Further details can be read in Reference 23.

D. Sample Positioning

Measurements were also made with a 4-grid retarding field analyzer to show that integration techniques automatically correct data for small misalignments of sample position (large misalignments could also be corrected if allowance is made for possible changes in solid angle detected and analyzer transmission). If a sample is not placed at the center of curvature of the grids, energy resolution is degraded and distorted spectral peak shapes result. This distortion results in errors in measurements made directly from $\mathcal{N}_m(E)$ or $\mathcal{N}_m^{(1)}(E)$ data but not in the Auger current value obtained on integration. An example of this is shown in Figure 6 where the energy distributions of electrons emitted from a cathode held at a potential of -300V are shown when the cathode is positioned at the center of curvature of the retarding field analyzer [Figure 6(a)], and the cathode is positioned off the axis of the retarding field analyzer and closer to it [Figure 6(c)]. It is quite obvious that a quantitative comparison between the two sets of data cannot be made directly from the $\mathcal{N}_m(E)$ distributions, but integration of the data recovers the cathode current value - compare the overall step heights of the integrated data in Figures 6(b) and (d).

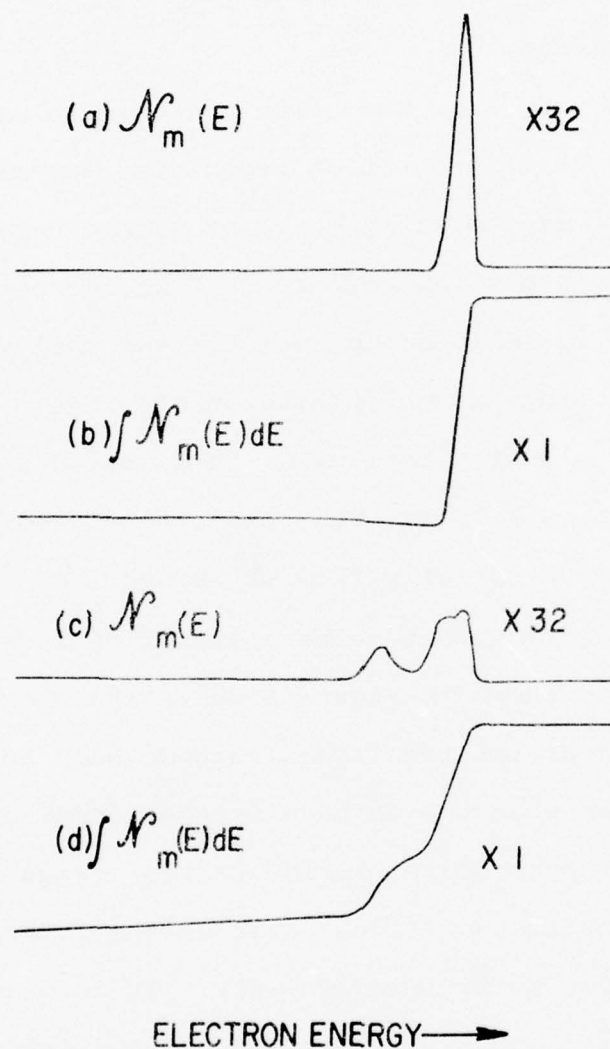


Figure 6 - Illustration of the application of integration techniques to correct for small sample misalignment using a retarding field analyzer.

Similar corrections would also apply to a cylindrical mirror analyzer, although the change in analyzer transmission with sample position is more critical.

E. Spectrum Subtraction Techniques

Most Auger spectrometers are designed to scan the electron energy range 0-2000 eV and, it is not always possible to find non-overlapping Auger peaks of the elements being studied, in this energy range. In such cases the presence of a particular element may be confirmed if its Auger signal strength is sufficiently large to produce significant amplitude changes in the appropriate part of the Auger spectrum of the other element. A good example of this is the detection of sulfur or carbon on ruthenium²⁴. Both sulfur and carbon Auger transitions overlap some ruthenium transitions but produce significant changes in the Auger spectrum when they are present in sufficient concentrations. This may be seen by comparing Figures 2(a) and 2(c) in Reference 24. Quantitative measurements of sulfur and carbon concentrations would be difficult however, because of the different Auger peak widths and line shapes of the individual overlapping Auger peaks. Relatively small concentrations of sulfur and carbon would probably go undetected.

In this contract spectrum subtraction techniques (SST) were developed and applied to (a) enhance the detection of small concentrations of elements where spectral overlap problems occur, and (b) retrieve Auger line shapes from high resolution Auger data where peaks from different elements overlap. SST could

also be applied to study the small changes in the fine details of Auger spectra due to changes in the chemical environment of surface atoms, the differences between two spectra being highlighted after subtraction. Chemical effects on spectra due to the presence of other elements may inhibit the application of SST to spectral overlap problems when dominant Auger transitions involve valence electrons, because of changes in spectral line shape. This would be most difficult when line shape changes were produced by the element whose spectrum was being isolated. Other potential applications for SST include subtraction of succeeding spectra from one another to follow changes during surface segregation, adsorption or sputtering treatments.

To obtain accurate subtractions of Auger data, the electron energy scale must be well established and reproducible. As the electron energy scale of most electron spectrometers depends on sample position, it is important that samples are always positioned at the same place with respect to the spectrometer, ideally at its focal point. Alignment of a sample to the focal point can be easily achieved by optimizing the signal measured from electrons that are elastically backscattered from the sample. In an earlier study of the segregation of sulfur on molybdenum it was pointed out that the detection of trace amounts of sulfur on molybdenum by Auger electron spectroscopy would be very difficult because of the almost complete overlap of the sulfur Auger peak near 150 eV with a molybdenum

Auger peak²⁵. The application of SST to this system greatly reduces this problem. An Auger spectrum from a molybdenum sample under study is shown in Figure 7(a). After the subtraction of an Auger spectrum from clean molybdenum taken with the same experimental parameters, Figure 7(b), a sulfur Auger peak was clearly observed, Figure 1(c), while the molybdenum Auger features were essentially eliminated. As the sulfur Auger signal was now isolated from the rest of the spectrum, its strength could be compared with a suitable standard for quantification or the sulfur Auger feature could be integrated twice to obtain a value for the sulfur Auger current.

Auger line shapes in high resolution derivative form data have often proved useful in obtaining information about the chemical form of surface constituents⁴. SST has also been applied to high resolution Auger data to determine line shapes by removing unwanted overlapping Auger features. This is illustrated in Figure 8 where part(a) shows that phosphorus and sulfur are present on molybdenum but their line shapes are masked by molybdenum Auger transitions. After subtraction of a corresponding high resolution molybdenum Auger spectrum, Figure 8(b), the phosphorus and sulfur Auger line shapes are obtained, Figure 8(c). This sulfur Auger line shape is quite similar to that observed on vacuum annealed stainless steel foils but is different from others such as on titanium and nickel.

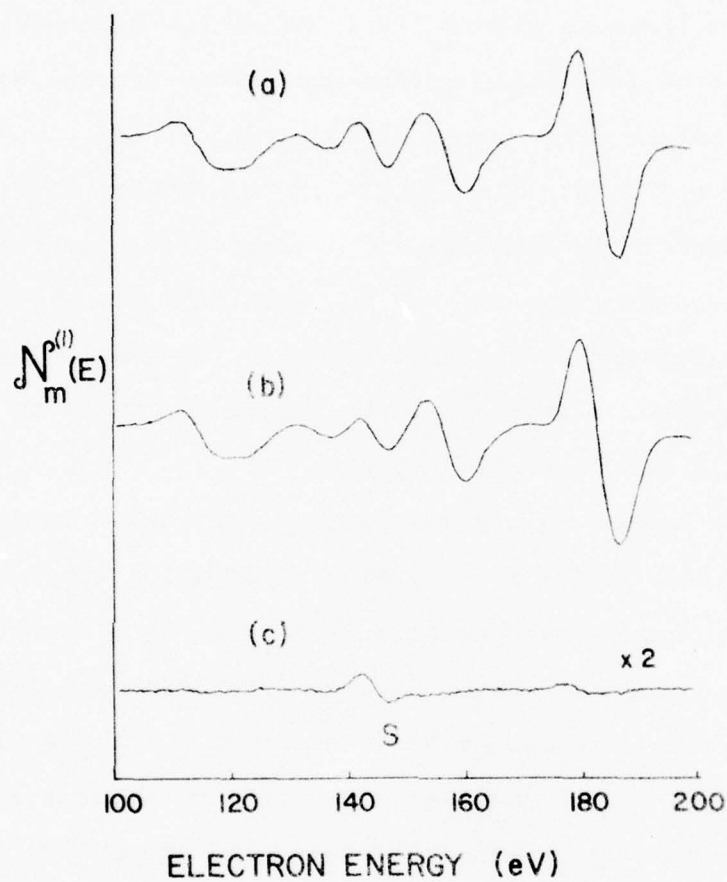


Figure 7 - Illustration of the application of SST to enhance the detection of sulfur on molybdenum.

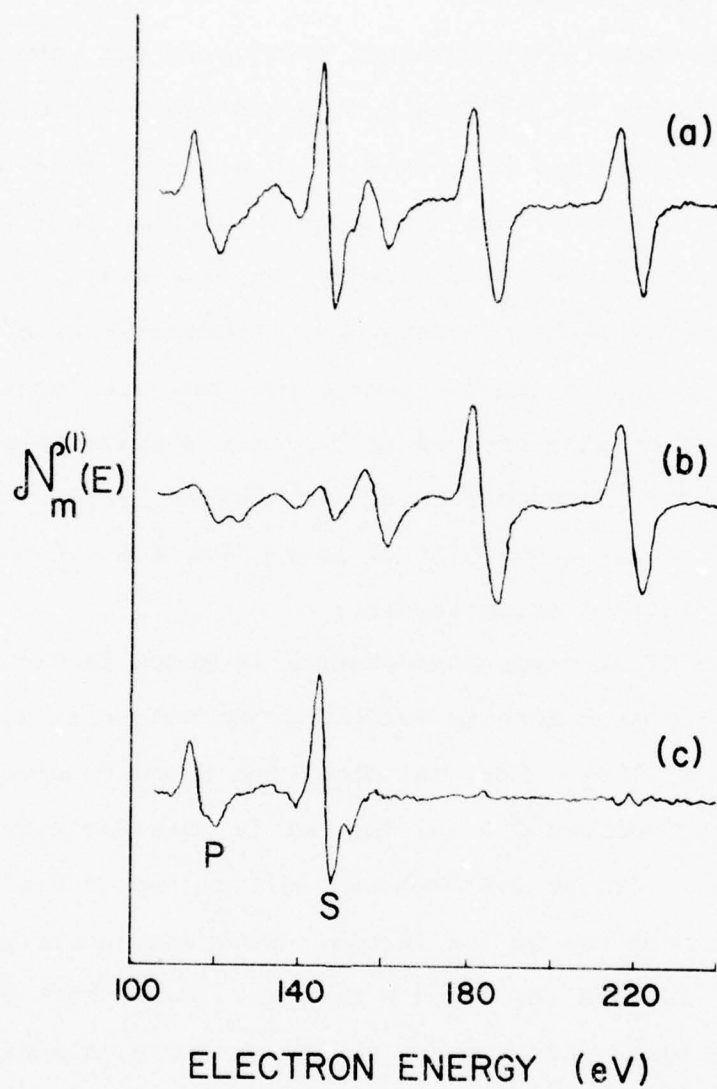


Figure 8 - Illustration of the application of SST to retrieve Auger line shapes.

F. Electron Beam Interactions

Most Auger spectra are obtained using electron beam excitation. Due to the use of finely focussed energetic electron beams (typically 3 μ A at 5 kV into a 15 μ m diameter spot) electron beam induced effects are not uncommon in studying many systems, especially those involving the adsorption of gases on metals or the detection of sodium on insulators. Electron beam effects are manifest in many forms but common problems are localized heating, the desorption of species from the surface being studied, beam induced decomposition of the surface being studied, and the beam induced adsorption of gases from the vacuum environment onto the surface being studied.

An example of electron beam effects is shown in Figure 9, being a study of such effects following the molecular adsorption of CO on Ni(110). Part (a) shows the C and O Auger spectra of freshly adsorbed CO, (b) the result obtained after an electron beam, 1.5 μ A at 1.5 keV, was left on for 10 min and (c) after the beam was on for 40 min. Note that quite pronounced changes occur in both the C and O spectra. For C both the main peaks and the lower energy peaks change markedly, almost all the features being replaced by new ones after 40 min interaction. At this stage the C Auger features resemble those of nickel carbide²⁶. Corresponding changes in the O Auger spectrum are less marked but nevertheless significant. The intensity of the feature on the high energy side of the main O peak decreases relative to that of the main peak, and the feature approximately 25 eV below the main peak is eventually replaced by two new ones

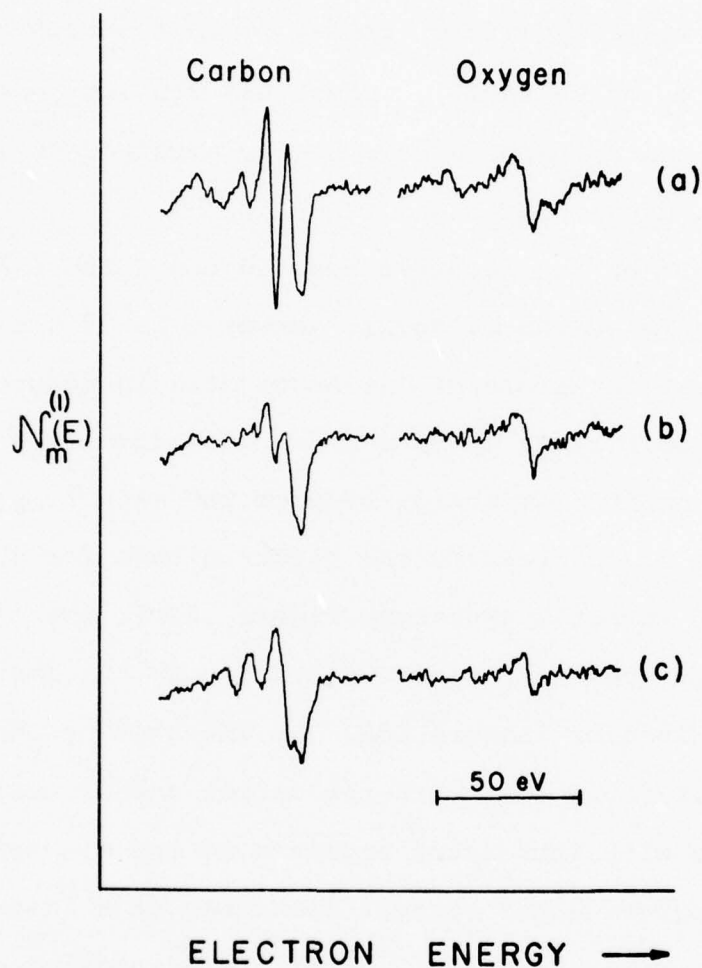


Figure 9 - First derivative Auger spectra of C and O on Ni (110): (a) following exposure of clean Ni(110) to 1×10^{-4} Pa of CO for 15 min; (b) after exposure to the electron beam for 10 min; (c) after exposure to the electron beam for 40 min. The electron beam was 1.5 μ A at 1.5 keV.

at the positions found for O_2 on Ni although they are not lucid in the data shown in Figure 9(c) (see also below). The O Auger spectrum obtained (from previously adsorbed CO) after 40 min interaction time is therefore similar to that obtained from the adsorption of O_2 on Ni(110)²⁷. These AES results indicate that the electron beam decomposes molecularly adsorbed CO into surface carbide and oxide.

The effects of the electron beam on the C and O Auger currents were also measured by double integration of the $\mathcal{N}_m^{(1)}(E)$ data. The first integrals of the Auger data in Figures 9(b) and (c) are shown in Figures 10(b) and (c) respectively. Note that the two peaks on the low energy side of the main O peak obtained after exposure of adsorbed CO the electron beam for 40 min are clearer in the integral spectrum, Figure 10(c), than in the raw derivative form spectrum, Figure 9(c), due to the improved signal/noise obtained on integration. By integrating the data of Figure 10 it is found that both the carbon and oxygen Auger currents decrease with increasing exposure to the electron beam, and that the oxygen Auger current decreases at a faster rate indicating disproportionation. After the adsorption of CO was shown from the Auger data that equal numbers of carbon and oxygen atoms were present on the Ni(110) surface²¹. The carbon and oxygen concentrations were found to decrease by 10% and 35% respectively after 10 min electron beam exposure, and by 30% and 90% after 40 min exposure.

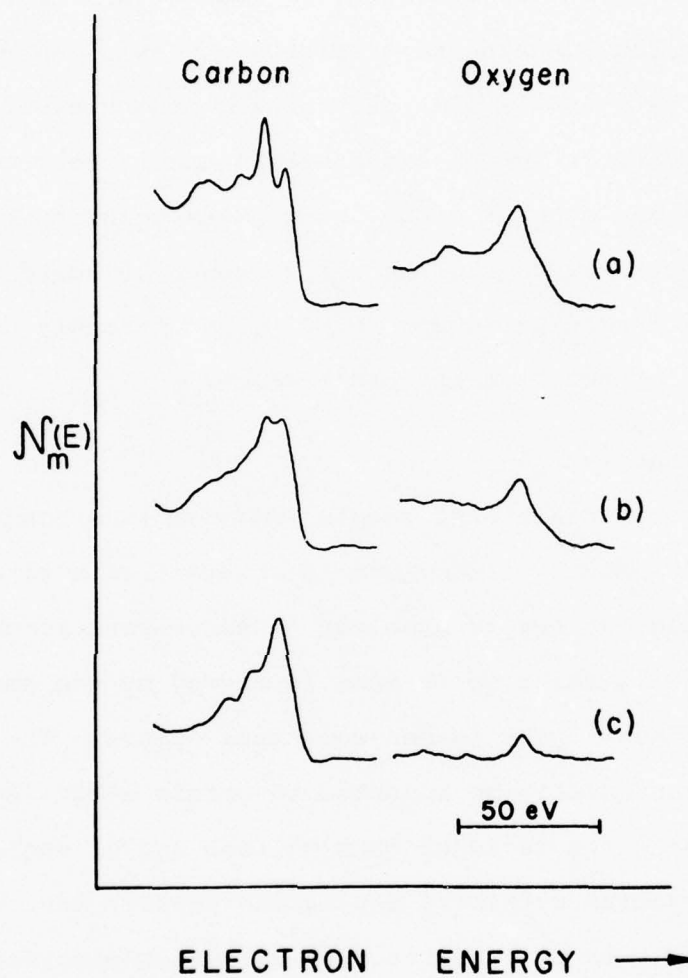


Figure 10 - First integrals of the respective data shown in Figure 9.

Experimental methods to reduce electron beam effects have been investigated in the contract, including (i) electron beam rastering (in the scanning Auger microprobe this can reduce beam effects by $\sim 500\times$), (ii) defocussing of the electron beam, and (iii) the use of low electron beam currents coupled with signal averaging spectra or by using pulse counting techniques. The use of soft X-rays (e.g. Mg K_{α}) to generate Auger electrons has also been investigated and found to be extremely useful in eliminating electron beam induced effects.

G. Sample Charging

In studying insulators, sample charging is a common occurrence. If the amount of charging is constant with time this generally causes no severe problems in Auger peak identification as all peaks will shift up or down in energy by the same amount. Distortion of Auger peak shapes sometimes occurs. The degree of charging can usually be adjusted to obtain useful Auger data e.g. by changing the incident beam voltage and/or angle of incidence. Even sodium activated insulating powders have been studied successfully in this contract by using low electron beam currents coupled with electron rastering techniques.

SECTION III

DEPTH PROFILING

A. Ion Gun Sputtering Rate Calibration

Two types of commercial ion guns were used in this contract for depth profiling, Physical Electronics Industries Models 04-161 and 04-191. Both guns were operated at ion energies of 2kV but as they were of different design they produced different ion currents even for the same electron emission currents in their ionizing chambers. Further, the focussed ion beam diameters are different and it was therefore decided to calibrate the sputtering rates for these two guns (at constant gas pressure) as a function of electron emission current. The ion guns were mounted on a Physical Electronics Industries model 545 system at standard distances from the samples to be sputtered. As tantalum oxide films can be grown on tantalum to reproducible thicknesses quite easily by anodization, they were chosen as a standard to measure the relative sputtering rates of the ion guns. The tantalum oxide films used here were anodized in phthalic acid at 80V, the thickness of the film being measured as 115nm by comparison with the sputtering rate of a 100nm standard supplied by Physical Electronics Industries. It should be mentioned that the changes in color of the films observed while sputtering provided a useful guide as to how much of the film had been sputtered away. The color contours also provided a measure of how well the ion beams were focussed.

The sputtering rates for tantalum oxide as a function of electron emission current (in the ion gun) are plotted in Figure 11 for argon at a pressure of 5×10^{-3} Pa (uncorrected nude ionization gauge reading). The time to sputter through the films was measured as the time taken for the oxygen Auger signal strength to decrease to 50% of its value in tantalum oxide. The ion guns were accurately aligned and focussed using the technique of ion excited Auger electron spectroscopy²⁸. Because of the relative ease of preparation and reproducibility of tantalum oxide film thicknesses, such films were usually mounted in the analysis chamber so that the sputtering rates of all materials investigated could be related to tantalum oxide and hence to each other. A list of such relative sputtering rates measured is provided in Table 1 for a number of materials - sputtering was carried out at 2kV with an argon pressure of 5×10^{-3} Pa.

The effect of anodization voltage on the thickness of tantalum oxide films was also studied by measuring the time required to sputter through the various films, Figure 12. It can be seen that the sputtering time increases linearly with preparation voltage. A study was also made to determine if the roughness of the tantalum substrates before anodization at 80V affected the measurement. Grinding the substrates with up to 25 μ m alumina particles before anodization was not found to affect the accuracy of the calibration measurements.

The use of xenon for sputtering was also studied for the model 04-161 ion gun. For tantalum oxide the sputtering rate was found to be 1.6 X that of argon at 2kV and 5×10^{-3} Pa (un-

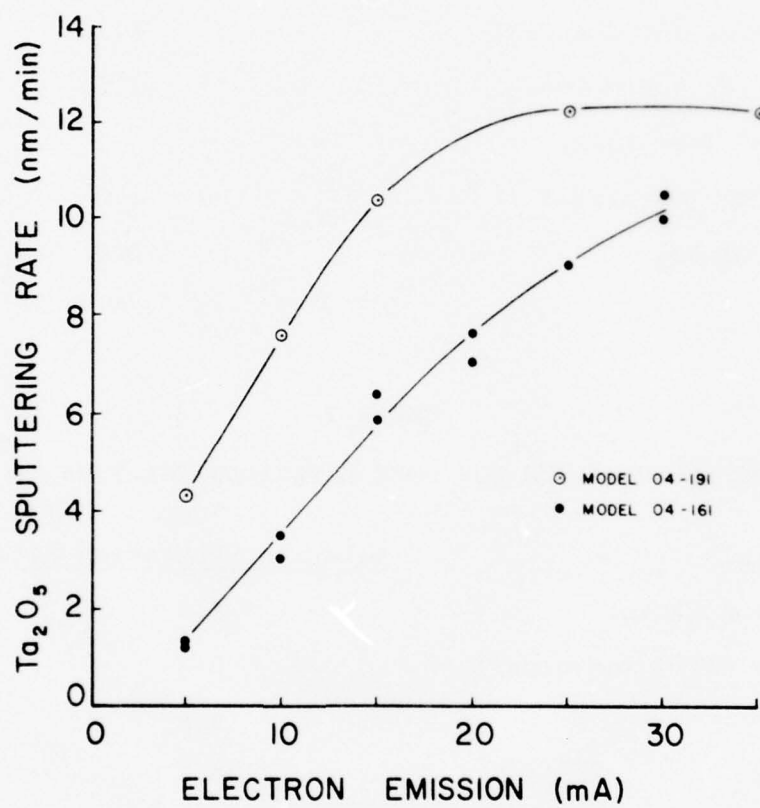


Figure 11 - Sputtering rate calibration curves for Ta₂O₅ films using model 04-161 and 04-191 ion guns.

TABLE 1

ARGON SPUTTERING RATES FOR SOME MATERIALS RELATIVE TO Ta_2O_5 .

<u>Material</u>	<u>Relative Sputtering Rate</u>
Al (on Ti)	1.4
Si_3N_4 (on Si)	0.9
SnO_2 (on CuInSe_2)	1.1
SiO_2 (on CuInSe_2)	1.6
WC (on glass)	1.1
TiC (on glass)	1.5
CuInSe_2	2.9

TABLE 2

XENON SPUTTERING RATES FOR SOME MATERIALS RELATIVE TO Ta_2O_5 .

<u>Material</u>	<u>Relative Sputtering Rate</u>
MoS_2 (on glass)	1.8
$\text{MoS}_2 + \text{Sb}_2\text{O}_3$ (on glass)	2.2
WC	0.9
TiC	0.8

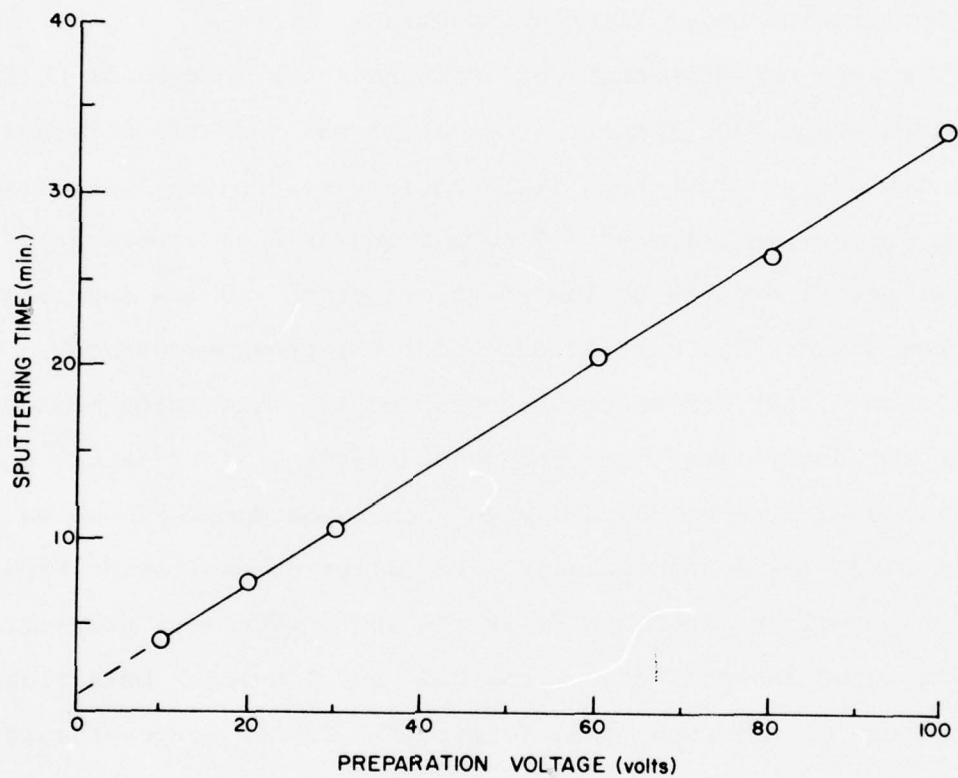


Figure 12 - Time required to sputter through Ta_2O_5 films as a function of anodization voltage.

corrected nude ionization gauge reading). This faster sputtering rate of xenon was often useful in studying thick films. Some sputtering rates relative to tantalum oxide, measured for xenon are listed in Table 2.

B. Ion Excited Auger Electron Spectra

The most common method for exciting Auger spectra of solids is by electron bombardment. However it was recently observed that low energy argon ions (2kV) could also produce Auger electrons in certain solids²⁹. A comparison of Auger spectra of Mg, Al and Si excited by low energy electron and low energy argon ion bombardment was carried out under the present contract. The most significant difference between the two excitation methods is in the Auger line shape produced. Typical Al LMM Auger spectra produced by electron and argon ion bombardment are shown in Figures 13 and 14 respectively. For electron excitation Figure 13, the main feature (labelled d) is due to $L_{2,3}VV$ Auger transitions. The features "a" and "c" are the 2nd- and 1st-order bulk plasmon losses of the main peak, feature "b" is the Coster-Kronig transition $L_1L_{2,3}V$, feature "e" the $L_{2,3}VV$ transition following initial double L level ionization. Note how the shape of feature "e" reflects essentially that of "d". With the argon excited spectrum, Figure 14, note the lack of Coster-Kronig and double ionization peaks from the spectrum. Note also the symmetric nature of the main Auger feature and the shoulder on its high-energy side. The energy at which this shoulder occurs is

essentially the same as that of the main Auger peak from electron excited Al. The symmetric feature in Figure 14 is interpreted as due to transitions from atomic-like M orbitals. Under ion bombardment Al atoms will be sputtered from the surface in excited states, and it is not unreasonable to expect Auger transitions to be detected from them also³⁰.

Under electron bombardment, Al L level ionization occurs through Coulomb excitation. Studies of ion-atom collisions show that inner-shell ionization can occur through an electron promotion mechanism³¹. During the collision a quasimolecule is formed and inner-shell electrons of the target (e.g., Al) may be promoted through molecular orbitals. If the distance of closest approach is sufficiently small such promoted inner-shell electrons may cross unoccupied outer levels in Ar^{+32} . After the collision, vacancies can therefore be left in the (originally promoted) inner-shells of the target (see Reference 31 for a detailed discussion of the mechanism). If one applies this mechanism to the case of ion-solid interactions, then for argon interacting with Al, ionization will take place in the $L_{2,3}$ levels of Al^{32} . One would then expect the argon excited Auger spectrum to consist primarily of a combination of $L_{2,3}^{MM}$ (atomic-like) Auger transitions from Al sputtered in excited states and $L_{2,3}^{VV}$ (bulk-like) Auger transitions from excited Al in the solid. To test this hypothesis, ion-excited and electron-excited Auger spectra were digitized and stored in a Nicolet instrument computer. The

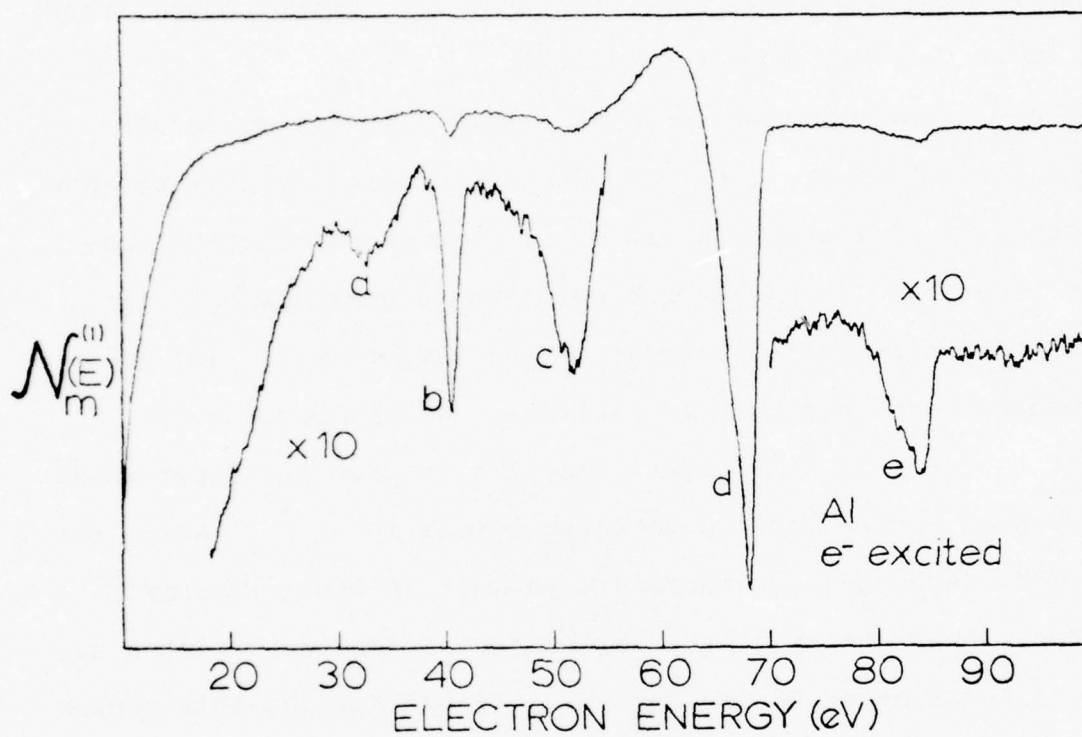


Figure 13 - Low energy Auger spectrum of Al excited by 2keV electron beam.

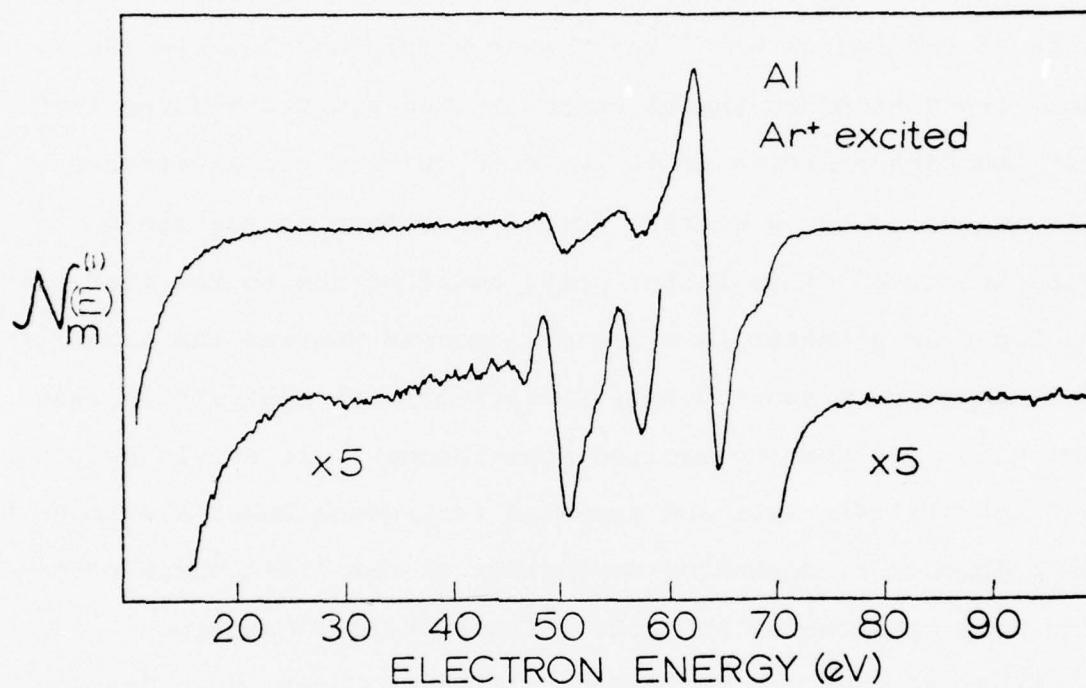


Figure 14 - Low energy Auger spectrum of Al excited by 3keV argon ion beam.

stored data are shown in Figure 15: (a) the electron-excited and (b) the ion-excited Auger spectra. Figure 15(c) shows the result obtained after subtracting a fraction of part (a) from (b), an essentially symmetric main peak together with some small features. Such a symmetric peak would be expected for atomic-like transitions. This subtraction procedure is only approximate because of the inclusion of the Coster-Kronig and "double ionization" transitions in the electron-excited spectra and the fact that the high-energy side of the main peak in the electron-excited spectrum has a sharper cutoff than that in the ion-excited spectrum. This latter point could be due to the fact that the ion-beam diameter is a few millimeters whereas the electron-beam diameter is about 0.2mm, resulting in an apparent degraded resolution for the ion excited measurements. It should be noted that not all materials are expected to produce Auger electrons by ion bombardment, depending on whether or not inner shell electrons can be promoted to produce inner shell ionization.

Studies of Mg and Si lead to similar conclusions. The ion excited signal (peak-to-peak) from Mg(2kV ions) is about an order of magnitude smaller than from Al. A study was also undertaken to compare the Mg $L_{2,3}$ MM Auger currents produced by low energy electron and argon ion excitation and it was found that under normal incidence a 1.5keV electron is only about a factor of 2 more effective than a 2keV argon ion in producing Mg $L_{2,3}$ MM Auger electrons. The ionization cross-section for the $L_{2,3}$ shell using 2kV argon ions was estimated as $1.5 \times 10^{-18} \text{ cm}^2$ per ion. Further

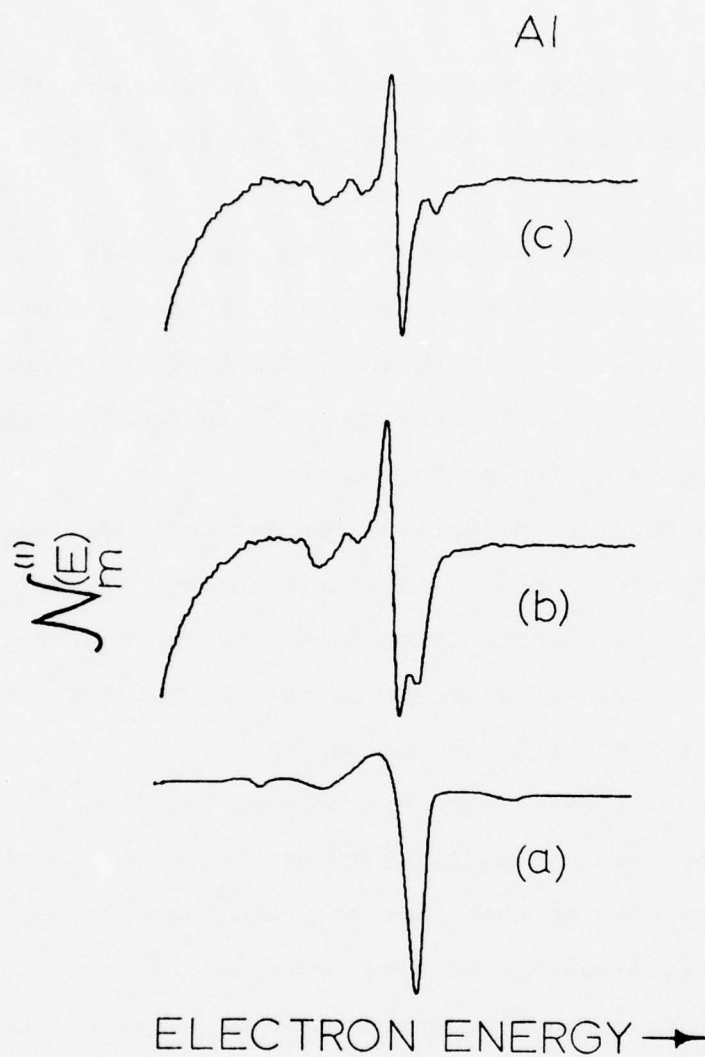


Figure 15 - Electron excited (part a) and ion excited (part b) Auger spectra of main Al features taken under identical experimental conditions. Part (c) shows the result obtained after subtracting a fraction of the electron excited spectrum from the ion excited spectrum.

details of this measurement can be read in Reference 33.

Other trends noted for ion excited spectra of Mg, Al and Si are:

(a) The ion excited Auger signal decreases with decreasing ion energy. This is consistent with the electron promotion model because as the ion energy is reduced, the distance of closest approach of the nuclei will increase, so the cross section for electron promotion will also decrease.

(b) At a given ion energy, the ion excited Auger signal decreases rapidly with increase in atomic number. This is also consistent with the electron promotion model because the $L_{2,3}$ binding energy increases with atomic number, thereby reducing the cross section for electron promotion.

(c) No transitions originating from an L_1 level are detected (this statement does not apply to Mg because of peak overlap). This is consistent with the electron promotion model as much higher ion energies would have to be used to reduce the internuclear distance in order to achieve promotion from an L_1 level (see Figure 4, Reference 34 for the case of Si). Further, no such transitions in Al were detected using 60 keV argon ions for excitation.³⁵

(d) No Auger transitions due to initial double L level ionization were detected using 3 keV argon ions for excitation. Such transitions have, however, been observed in Al using 60 keV argon ion bombardment.³⁵

(e) Bulk plasmon losses associated with the $L_{2,3}VV$ Auger transitions are observed for the ion excited spectra, 2nd-order

losses are seen for Mg and Al, while 1st-order losses are seen for Si. 1st order losses for Mg and Al overlap with other peaks. This result contrasts with other interpretations of ion excited Auger spectra^{35,36} where no structure was assigned to plasmon losses due to an apparent discrepancy between known plasmon loss energies and observed peak positions. No such discrepancy exists, however, when ion excited spectra are interpreted in terms of a combination of atomic-like and bulk transitions.

Further details of this work can be read in References 29, 30 and 33.

1. Application to ion gun alignment

In order to obtain reliable depth profiles with Auger electron spectroscopy it is of paramount importance that the ion gun beam, electron beam and specimen be accurately positioned to coincide at the focal point of the analyzer used, typically a cylindrical mirror analyzer (CMA).²⁸ Most procedures used were tedious involving the use of a Faraday cup or trial and error techniques. However, the phenomenon of low energy ion excited Auger spectroscopy can be used to provide a rapid method for ion gun alignment, and to check alignment at any later time. (Realignment was sometimes found necessary, probably because of small movements between ion gun components due to thermal effects).

This technique was developed in conjunction with R.W. Springer and T. W. Haas and is based on measuring the ion excited LMM signal



Figure 16 - Example of precise ion gun alignment using ion excited Auger spectroscopy. Magnification 20X.

from a small dot of Al (about 1.5mm in diameter) evaporated onto a material such as Cu that does not produce a significant ion excited Auger signal under 2kV argon ion bombardment. The technique is accurate and is discussed fully in Reference 28. An example of the accuracy of the technique is shown in the absorbed current image of a specimen after profiling, Figure 16. The small bright central region is the ion bombarded area. The specimen shows through a circular aperature (which appears as a black ellipse) in a specimen mount. (The specimen was mounted at an angle to the electron beam, hence the elliptical shape of the aperature).

2. Interference during depth profiling

During depth profiling studies of Mg, peaks due to argon ion excited $MgL_{2,3}$ MM Auger transitions were sometimes observed superimposed on the electron excited $MgL_{2,3}$ MM Auger transitions. This effect could be detected because the Auger line-shapes are different for these two methods of excitation,³⁰ and the fact that the $MgL_{2,3}$ ionization cross section using 2 keV argon ions is similar to that using 1.5 keV electrons³³. (These beam energies are typical of those used in depth profiling). A typical result obtained from Mg is shown in Figure 17, (a) being the Auger spectrum excited by argon ions, (b) that excited by electrons and (c) the result obtained with both beams on simultaneously. The sum of the signals in Figures 17(a) and (b) is shown in Figure 17(d) and is not significantly different from that obtained with both beams on simultaneously.

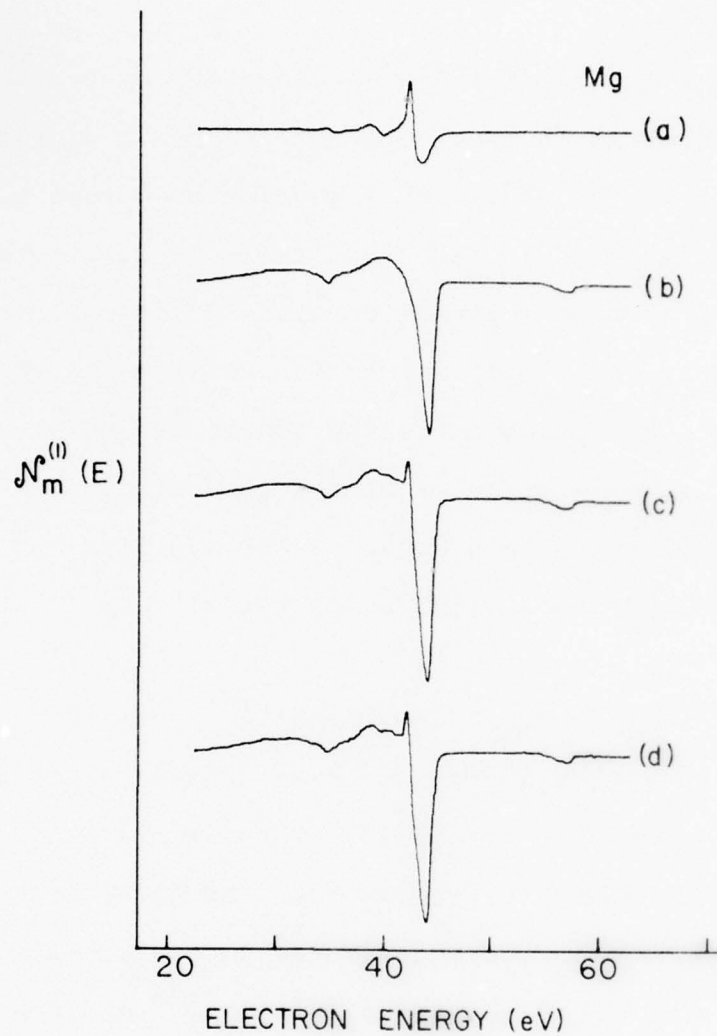


Figure 17 - LMM Auger spectra of Mg taken (a) with a 10 μ A, 2000 eV argon ion beam, (b) with a 6 μ A, 3000 eV electron beam and (c) with these two beams on simultaneously. Part (d) is the sum of the data shown in (a) and (b).

The contribution of the ion excited Auger signal to the measured peak-to-peak height, 20% in Figure 17, can be a source of error in depth profiling Mg. The signal strength due to Ar^+ can be decreased most effectively by using a lower ion beam energy as the signal strength varies rapidly with ion energy in the keV range.³⁰ Use of higher bombardment energies would enhance the contribution of the ion excited Auger signal. Further reduction of the effect could be accomplished by using lower ion currents or larger electron beam currents, as dictated by desired sputtering rates or by possible heating of the specimen under study. Alternately, it may be possible to use the less intense MgKLL Auger peaks (near 1200eV) for depth profiling as these transitions are not excited by low kV ions, but this would require a higher electron beam energy for efficient KLL Auger production. Another problem arises in depth profiling Mg compounds as for example no ion excited signal is detected from MgO.

Other metals can also give rise to Ar^+ excited Auger transitions but of all metals studied to date, Mg appears to give the largest Auger signal strength under Ar^+ impact³⁰. Auger transitions can also be excited in metals under low energy (<5keV) impact with other ions but such effects were not widely studied.

C. Electrostatic Shielding of Ion Guns

Two problems were noted in operating the commercial ion guns

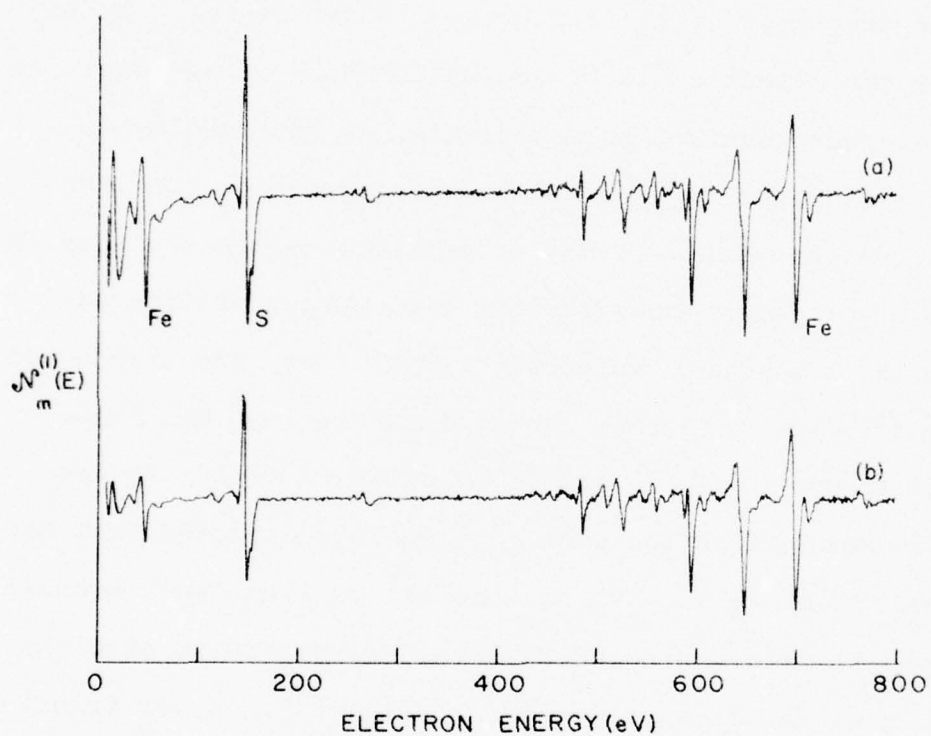


Figure 18 - Auger spectra of a flashed stainless steel specimen taken (a) with the ion bombardment gun off and (b) with the high voltage (2000 V) applied to the ion gun.

as supplied by the manufacturer, due to the fact that they were not electrostatically shielded: (a) a reduction in signal strength of low energy Auger features relative to those at higher energy, and (b) an error in measuring the beam currents when applying a bias to the sample. An Auger spectrum of a flashed stainless steel specimen taken in a scanning Auger microprobe³⁷ system is shown in Figure 18(a). The major features due to sulfur and iron Auger transitions are indicated on the figure. Application of 2000 V to the ion bombardment gun (in vacuum) caused the Auger spectrum to change to that shown in Figure 18(b) and it can be seen that the Auger peaks have decreased in size and by varying amounts, the decrease being larger the smaller the Auger energy - the low energy Fe peak decreased by more than 50%, the sulfur peak by 35% and the high energy Fe peak by about 10%. As the decreases in signal size are due to electrostatic effects from the ion gun, the magnitude of the decrease depends on specimen geometry with respect to the ion gun and spectrometer. The data shown in Figure 18 were obtained using a 0.73 μ A, 5000eV primary electron beam and there was no detectable change in the beam position on the specimen at a magnification of 500 X. The beam current was measured using a Faraday cup. A current of 0.71 μ A was obtained by applying a +97 V bias to the metallic specimen and measuring the current to ground. This latter method is commonly used to measure beam currents but is also subject to errors if current measurements are made during depth profiling

with an unshielded ion gun. In this case the electron current then measured 0.66 μ A, the decrease being due to the loss of some secondary electrons caused by the electrostatic field from the ion gun. Effects of unshielded ion guns on Auger peak heights were observed in other Auger systems also, the size of the effect depending on the geometries of the systems.

These problems due to unshielded ion guns were overcome by enclosing the ion gun in a stainless steel shield. The shield covered the complete length of the ion gun and was attached to the vacuum chamber due to the rather small clearance of the ion gun vacuum port. No significant problems were now encountered in measuring Auger signal strengths or in measuring beam currents.

D. Some Other Problems in Depth Profiling

There are many other problems³⁸ associated with depth profiling using Auger electron spectroscopy such as (a) non-uniform ion flux, (b) microscopic roughness of the target produced by the ion beam, (c) ion induced motion of impurities, (d) surface damage by the ion beam, (e) preferential sputtering for compounds and (f) sample charging. The non-uniformity of the ion flux is usually not a serious problem if small electron beams are used for Auger excitation. A set of deflectors was constructed for the model 04-161 ion gun to allow ion beam rastering if such a problem arose. The newer model 04-191 ion guns are

equipped for rastering by the manufacturer. Roughness produced by the ion beam can be quite serious but it depends on many factors such as crystallinity the angle of the ion beam relative to the surface being bombarded and the presence of foreign particles on the specimen. Many compounds can decompose under low energy argon ion bombardment e.g. in reducing oxides to the corresponding metal or a lower oxide³⁹. Other aspects of these problems can be read in Reference 38.

An example of sample charging during depth profiling is illustrated in Figure 19 for a glassy material. The Auger spectrum shown in Figure 19(a) is from the glassy material before ion bombardment. When the ion beam (2kV, 3mA electron emission, 5×10^{-3} Pa argon, model 04-161) was turned on the spectrum shown in Figure 19(b) was obtained. It can be seen that the KLL oxygen and aluminum peaks have shifted down in kinetic energy and have also decreased in size. The degree of shift indicates that the sample charged to about +200V on application of the ion beam. It was found that applying a voltage of -200V to the sample mount during sputtering cancelled out the effects of charging on the oxygen and aluminum KLL peaks, Figure 19(c). Note that not only have the peaks returned to their approximate energies before ion bombarding, but that the peak intensities are also close to their correct values. As the degree of sample charging usually changes during ion bombardment, it may be use-

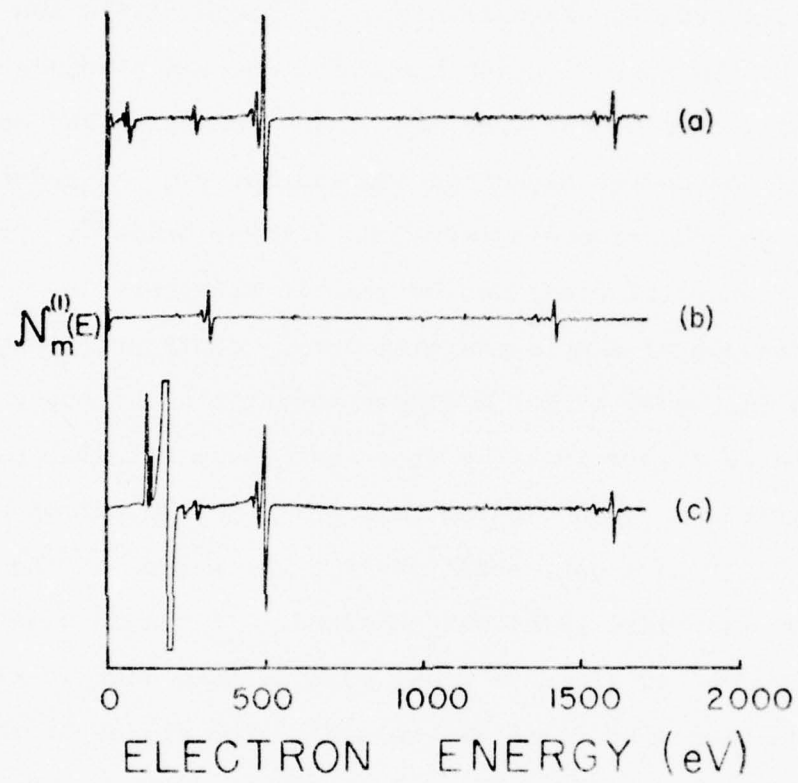


Figure 19 - Illustration of the effect of sample charging due to ion bombardment.

ful to design a system to automatically compensate for the sample charging to allow accurate depth profiles to be obtained for such samples.

The effect of substrate roughness was also investigated for the case of copper films on aluminum. 20nm evaporated Cu films on one polished and several rough Al substrates (prepared with 600, 400, 280, and 120 grit silicon carbide papers) showed similar thicknesses on depth profiling. However, after sputtering through the Cu films, the Al KLL substrate signal (near 1400 eV) did not increase rapidly for the roughened substrates, in contrast with the increase obtained from the polished substrate. In depth profiling, the depth resolution is usually about 5-10% of the depth of material removed.

Another problem encountered in depth profiling was the signal-to-noise limitation imposed by the multiplex system supplied with the scanning Auger microprobe³⁷. The signal-to-noise for depth profiling was improved by modifying the multiplexer to allow the use of longer time constants in the phase sensitive detector, a time constant of 3s being found suitable in most cases where small Auger signals had to be measured. Further details can be read in Reference 40. A control panel was also added to the multiplexer to add 'SKIP' or 'PLOT' operation.

E. The Application of Tailored Modulation Techniques to Depth Profiling

In profiling through thin films of aluminum and silicon ox-

ides on the pure materials large energy shifts in the Auger transitions occur in going from the oxide to the substrate. For Al metal the main LVV and KLL peaks occur at 67eV and 1396eV respectively whereas in Al_2O_3 they occur at 52eV and 1389eV⁴¹. Because of these shifts depth profiles of Al_2O_3 on Al are often plotted using the two LVV peaks or the two KLL peaks separately⁴² and provide information about changes in chemistry with depth, but do not provide useful information about aluminum concentrations near the interface. Depth profiles of the same system using wider energy windows to encompass peaks in both the oxide and the metal show little improvement for quantitative analysis; in fact the use of such peak-to-peak height measurements incorrectly indicate a depletion of aluminum near the Al_2O_3 -Al interface.⁴³

A conventional depth profile of Al_2O_3 on Al using peak-to-peak heights in $\mathcal{N}_m^{(1)}(E)$ of the O KVV and Al $\text{KL}_{2,3}\text{L}_{2,3}$ transitions is shown in Figure 20. From this profile it can be seen that the measured Al Auger signal strength decreases soon after the commencement of sputtering, passes through a minimum at which the Al signal strength is about one half of that before sputtering, and then increases towards a new value which is slightly bigger than that obtained before sputtering. The oxygen Auger signal strength decreases slowly at first and then rapidly decreases towards zero as the Al_2O_3 is removed. From such a profile it is difficult to determine where the Al_2O_3 - Al boundary

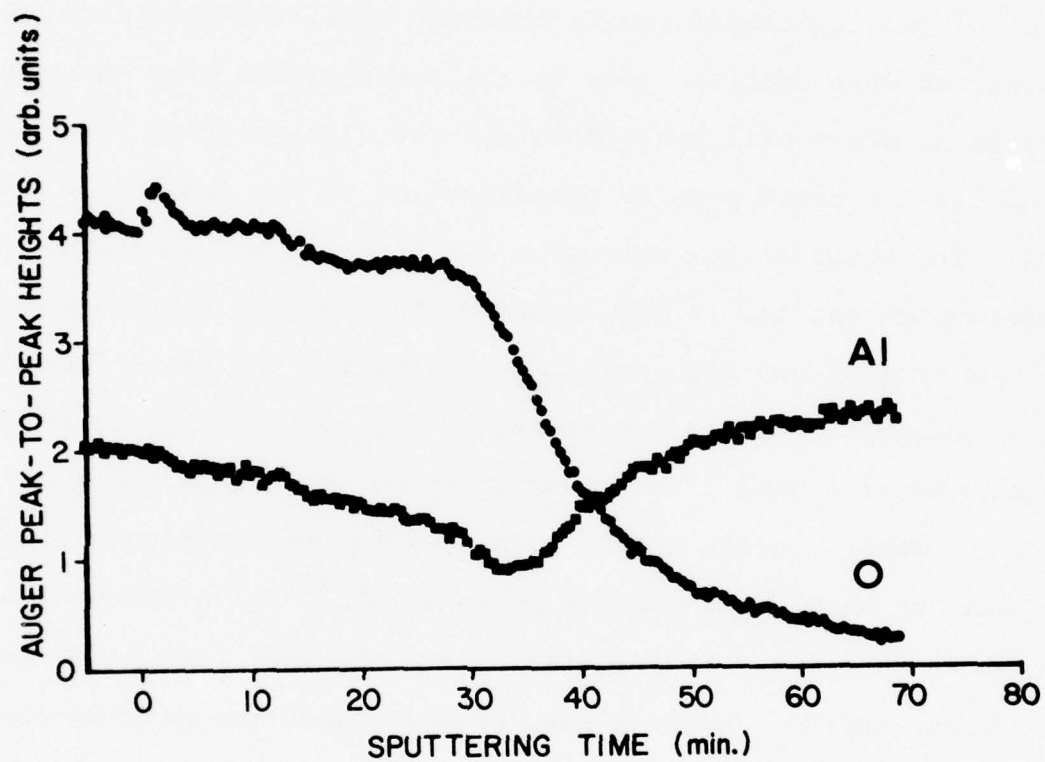


Figure 20 - Depth profile of Al₂O₃ on Al obtained using peak-to-peak heights in first derivative spectra $N_m^{(1)}(E)$.

is, the best estimate probably being made by noting where the oxygen signal strength decreases to one half its initial value. The Al profile certainly does not follow that expected from the variation in Al atomic densities in Al_2O_3 and Al metal. As the Al atomic density is about 40% higher in Al metal than Al_2O_3 , the Al density should remain constant until the interface is approached when contributions to the Auger signal from the underlying Al metal will cause the measured Al density to increase, and finally reach a value corresponding to the density in pure Al. The Auger signal strengths are not expected to follow this dependence exactly as the escape depths for the KLL Auger electrons from Al and Al_2O_3 are not necessarily the same - the bigger the escape depth, the larger the volume contributing to the measured Auger signal. The reason for the unusual behavior of the Al KLL depth profile can be seen by reference to Figure 21 which shows the Al $\text{KL}_{2,3}\text{L}_{2,3}$ Auger peaks in $\mathcal{N}_m^{(1)}(\text{E})$ after various sputtering times. Figure 21(a) shows the peak from Al_2O_3 before sputtering. After 5 min, Figure 21(b), the peak-to-peak height has decreased slightly but no new features are seen. After 20 min, Figure 21(c), the signal size has further decreased but now a new peak is resolved on the high energy side. This new peak is due to the $\text{KL}_{2,3}\text{L}_{2,3}$ transitions from Al metal and is at an energy 7 eV higher than the $\text{KL}_{2,3}\text{L}_{2,3}$ transitions from Al_2O_3 . With further sputtering the Auger peak-to-peak height

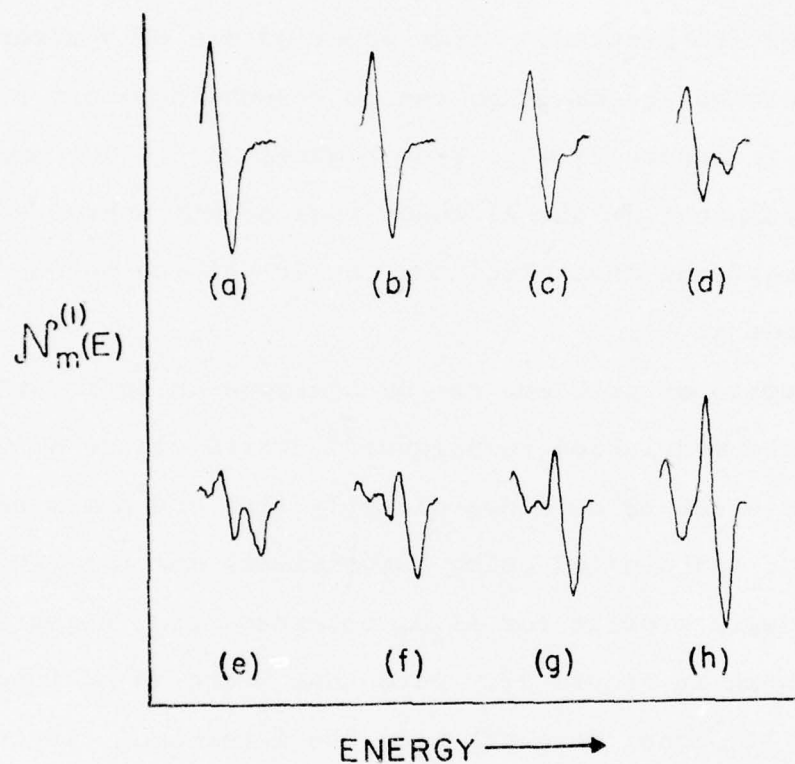


Figure 21 - First derivative Al $KL_{2,3}L_{2,3}$ Auger spectra from Al_2O_3 on Al after sputtering for various times: (a) before sputtering; (b) 5 min; (c) 20 min; (d) 30 min; (e) 33 min; (f) 37 min; (g) 40 min; (h) 65 min.

from Al_2O_3 continues to decrease while that from Al metal increases. During depth profiling the energy window for the Al signal was set wide enough to encompass the peaks from both Al_2O_3 and with the multiplexing equipment the difference between the maximum positive and negative going peaks within the energy window are plotted. After about 33 min of sputtering the Al signal reached its minimum, the corresponding Auger spectrum being shown in Figure 21(e). From Figures 21(f), (g) and (h) it can be seen that as the Al Auger peak grows, a new peak on its low energy side does also, the latter peak being due to bulk plasmon losses in Al.

These sorts of problems can be overcome in depth profiling using tailored modulation techniques⁴⁴, where measures of the Auger currents can be obtained directly from the phase sensitive detector and plotted using conventional multiplexing equipment. The depth profile for Al_2O_3 obtained using Auger area values is shown in Figure 22. Note that there is no longer any decrease in Al signal strength near the interface. In fact, the Al signal is seen to increase slowly after sputtering for about 20 min and this corresponds to where Al metal was first clearly detected in $\mathcal{N}_m^{(1)}(E)$. As the interface is approached the Al signal further increases due to the increased atomic density of Al. Also the interface is more clearly defined, the Al signal increasing by half its total increment at approximately the

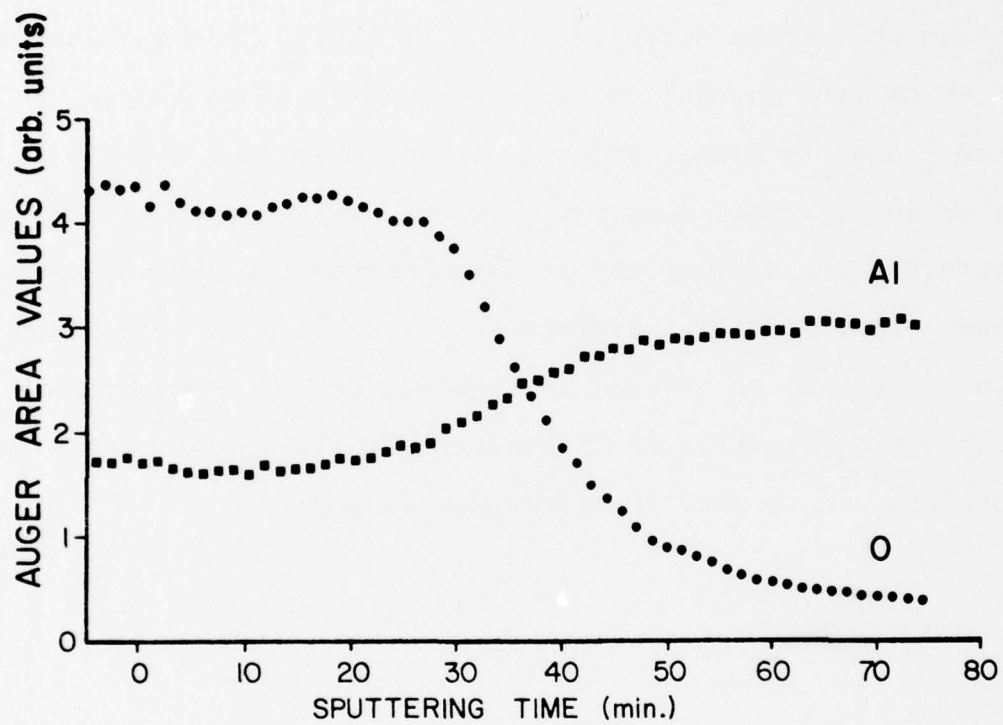


Figure 22 - Depth profile of Al₂O₃ on Al using Auger area values obtained with TMT.

same time as the oxygen signal decreases to half its original height, about 36 min. The depth profile shown in Figure 22 was obtained by integrating over an energy range of 35 eV and for this energy range the Al signal increased by about 75% in going from Al_2O_3 to Al metal. As mentioned earlier the change in Al signal strength depends somewhat on the energy range of integration due to the different electron energy loss mechanisms and these loss mechanisms would need to be known before the measured change in signal strength could be related exactly to the change in Al atomic density. However, in cases where the loss mechanisms are similar and no large changes in backscattering occur, e.g., $\text{Ti}/\text{TiO}^{45}$, differences in Auger area values should relate directly to changes in atomic density. Further details about the application of tailored modulation techniques to depth profiling can be read in References 46 and 47.

SECTION IV

OTHER SURFACE ANALYSIS TECHNIQUES

Some other techniques were also studied to varying degrees to complement Auger analysis. These techniques are soft X-ray appearance potential spectroscopy (APS), secondary ion mass spectroscopy (SIMS) and X-ray photoelectron spectroscopy (XPS).

A. Soft X-ray Appearance Potential Spectroscopy

Soft X-ray appearance potential spectroscopy (APS) is perhaps the simplest method for measuring core electron binding energies of solids. The solid is bombarded with monoenergetic electrons of variable energy and the total X-ray emission intensity is monitored, threshold behavior in the X-ray emission corresponding to the onset of core level excitations. Although the onset of these additional X-rays can be quite sudden, the additional intensity is small compared with the background X-ray intensity due to Bremsstrahlung radiation, making direct measurements of electron binding energies rather difficult⁴⁸. Experimentally, this difficulty has been overcome by using potential modulation and phase sensitive detection techniques enabling measurements of the first or second derivatives of the total X-ray emission intensity to be made⁴⁹. By taking such derivatives the slowly varying background X-ray intensity can be eliminated, while the sudden threshold behavior is enhanced and can be amplified al-

allowing for easier measurements of the core electron binding energies. To date, most measurements have been made for binding energies below 1000 eV and as the mean free path for inelastic scattering in solids for electrons in this energy range is less than about 2 nm, APS probes the surface regions of solids allowing identification of certain elements in those regions. Elements reported to produce good APS spectra so far have been listed in a periodic table⁴⁹.

With certain assumptions, the (near threshold) excitation cross section in APS is proportional to the self-convolution of the density of empty states above the Fermi level⁴⁸. For the 3d transition metals the Fermi level usually lies within a relatively sharp, structured d-band which is superimposed on a broad free-electron-like 4s band. If such a conduction band is represented by a series of rectangular functions, the self-convolution is a series of ramp portions, and its derivative would consist of a peak, a somewhat smaller undershoot and a step for each core level excited⁴⁸. Indeed, such first derivative APS peaks have been observed for the 3d transition metals, the width of the peak decreasing with atomic number corresponding to the filling of the 3d band⁵⁰. In Cu, the d band is full and no peak is observed⁵¹. The shapes and heights of these peaks are affected by oxidation and provide useful information about unoccupied energy states⁴⁹.

1. Quantitative aspects

Although the derivative APS peaks of the 3d transition metals have been catalogued, their relative signal strengths had

not been reported. In this contract the relative L_3 and L_2 soft X-ray appearance potential spectroscopy signal strengths were measured for pure Ti, V, Fe, Co, Ni and Cu using a gold plated photocathode detector. The peak-to-peak signal strengths obtained from high resolution dI/dE data vary markedly between elements, with no peak being found for Cu, Figure 23. (dI/dE is the first derivative of the measured collector current). These signal strengths could be used as a basis for semi-quantitative analysis of Ti, V, Fe, Co and Ni, but not of Cu as it gives no peak. For an accurate determination of the concentration of one of these elements at a particular surface, its APS peak shape would have to be identical to that of the metal or some standard, but this is often not possible as changes in the density of states of the unfilled 3d band due to different chemical environments are reflected in the APS peak shape⁴⁹.

In an earlier APS study undertaken to resolve apparent discrepancies between the sensitivities of APS and AES to Ti and O, it was shown that if the APS signal strengths were measured away from threshold, rather than by measuring the threshold peak-to-peak signal strengths, such discrepancies were removed⁴⁵. In the case of the 3d transition metals, one would then be measuring the APS signal strength from the unfilled density of states of the free-electron like 4s band, and would not be subjected to the effects of the structured 3d band. In a first derivative APS spectrum, the signal due to the unfilled 4s states appears as

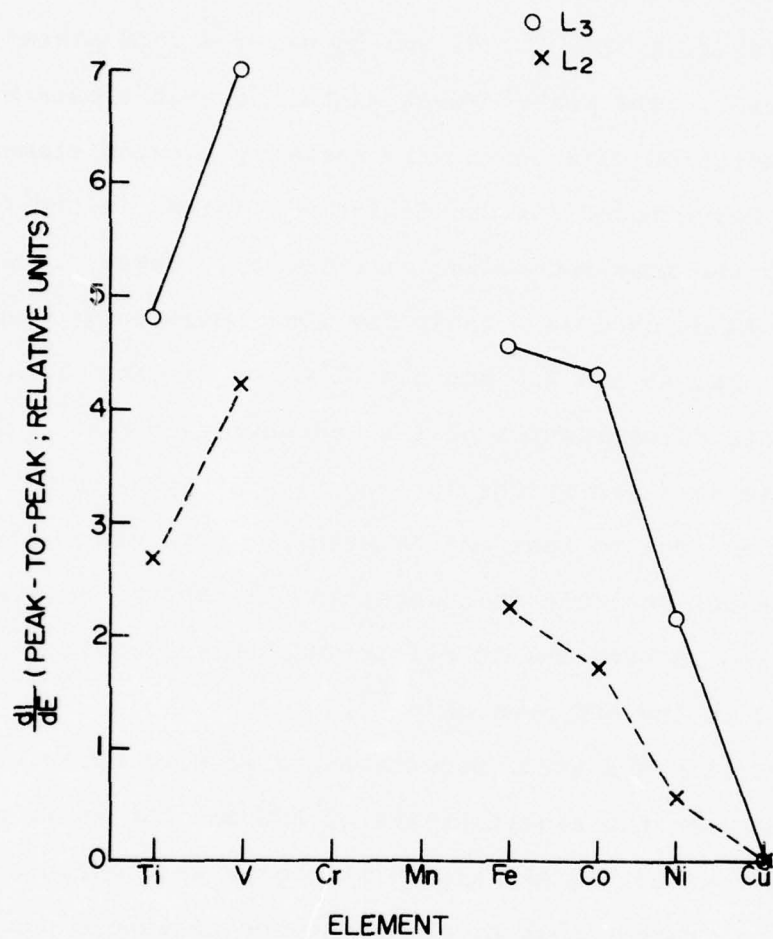


Figure 23 - Relative L₃ and L₂ APS signal strengths of Ti, V, Fe, Co, Ni and Cu measured as the peak-to-peak deflections of their first derivative spectra. No peaks were detected from Cu.

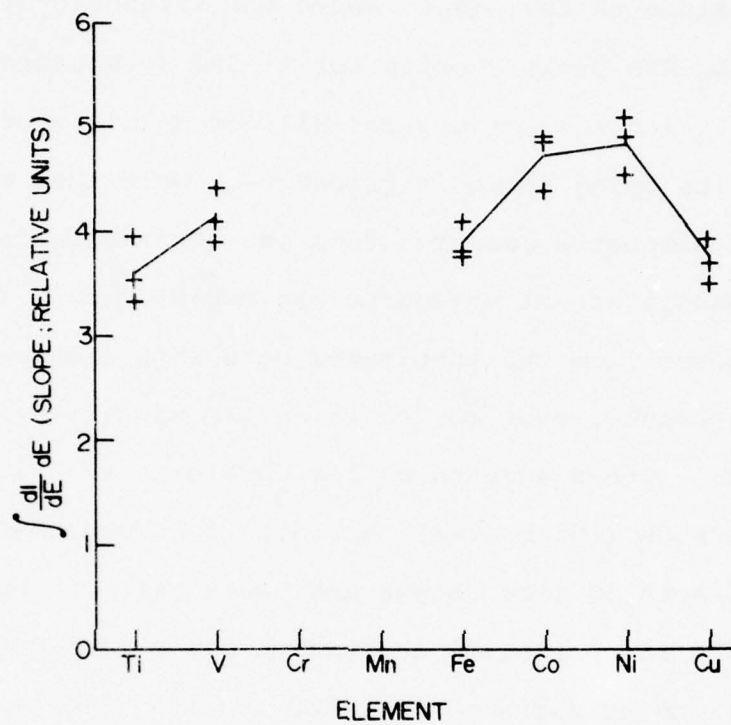


Figure 24 - Combined L_3 and L_2 APS signal strengths from Ti, V, Fe, Co, Ni and Cu measured using integration techniques.

a small increase in the dc signal level relative to that before threshold. This small change in dc signal level can best be measured by integrating the derivative data once, and then measuring the slope of the signal above the threshold structure. As the L_3 and L_2 APS peaks overlap for Ti and V, measurements of the combined (L_3 and L_2) offsets for all the metals studied were made, the results being shown in Figure 24. Note that whereas the APS signal strengths measured from the derivative data showed large variations in signal strengths between elements, signal strengths measured from the integrated data show little variation between elements, even for Cu which had no peaks in the derivative data. Other advantages for obtaining APS signal strengths from such (integrated) data are: less dependence due to chemical effects on line shapes and the simple correction of signal strengths for potential modulation distortion, as had already been applied to corresponding AES studies (see Section IIA).

Measurements of the relative L_3/L_2 signal strengths were also made in this contract. The ratios obtained from peak-to-peak heights of the derivative data are listed in Table 3 and compare favorably with similar measurements reported earlier for the 3d transition metals⁵⁰. No peak-to-peak measurements were possible for Cu due to the lack of peaks at threshold. It can be seen that ratios obtained in this manner deviate from the expected intensity ratio of 2 based on the statistical weighting

$2j + 1$ ⁵⁰. Some of this deviation is due to the method of measurement, the L_3 and L_2 peaks overlapping for the lighter atoms and their having different line-widths for the heavier atoms⁵⁰. The selection rules for the radiative decay of 2p holes may also be j -dependent⁵². In this work, integration has been applied to measure the L_3/L_2 signal strength ratios for Ni and Cu from the near threshold slopes of the integrated spectra. For these two metals the L_3 and L_2 thresholds are well separated allowing accurate measurements to be made by integration. For both Ni and Cu the L_3/L_2 signal strength ratios measured from the above-threshold slopes are approximately 2. Further details of these quantitative aspects of APS can be read in Reference 53.

TABLE 3

L_3/L_2 APS SIGNAL STRENGTH RATIOS FOR SOME 3d TRANSITION METALS OBTAINED FROM PEAK-TO-PEAK HEIGHT MEASUREMENTS IN FIRST DERIVATIVE APS SPECTRA.

Metal	L_3/L_2 ratio
22 Ti	1.8
23 V	1.7
26 Fe	2.0
27 Co	2.5
28 Ni	3.9
29 Cu	^a

^aCannot be measured from first derivative APS spectrum.

2. Comparison with Auger electron spectroscopy

One problem encountered during the contract was the detection of Mn in 1.4% Mn steel using Auger electron spectroscopy.

The problem was due to the fact that the main Mn and Fe Auger peaks overlap almost completely prohibiting the direct detection of such small concentrations of Mn. When spectrum subtraction techniques were applied to the Auger data, however, the Mn Auger features were readily resolved and the surface concentration of Mn was estimated as 1.7% using standard Auger sensitivity factors.¹

APS is a useful technique for studying the first row of transition metals and was therefore applied to this same system for comparative purposes. APS measurements indicated that the surface concentration of Mn was about 2.0% in close agreement with the Auger result. It should be mentioned that the APS data were obtained using an electron emission current of 2mA. The use of larger emission currents, e.g. 4mA, caused Mn to segregate to the surface. APS then showed a surface concentration of about 6% Mn, which was confirmed by subsequent Auger analysis which showed 5.5% Mn.

B. Secondary Ion Mass Spectroscopy

An energy filter was constructed and mounted on an existing quadropole residual gas analyzer to enable secondary ion mass spectroscopy (SIMS)⁵⁴ measurements to be made in the scanning Auger microprobe system. The dynode-type electron multiplier was also replaced by a channeltron-type for better amplification. The channeltron was mounted on axis and phase sensitive detection

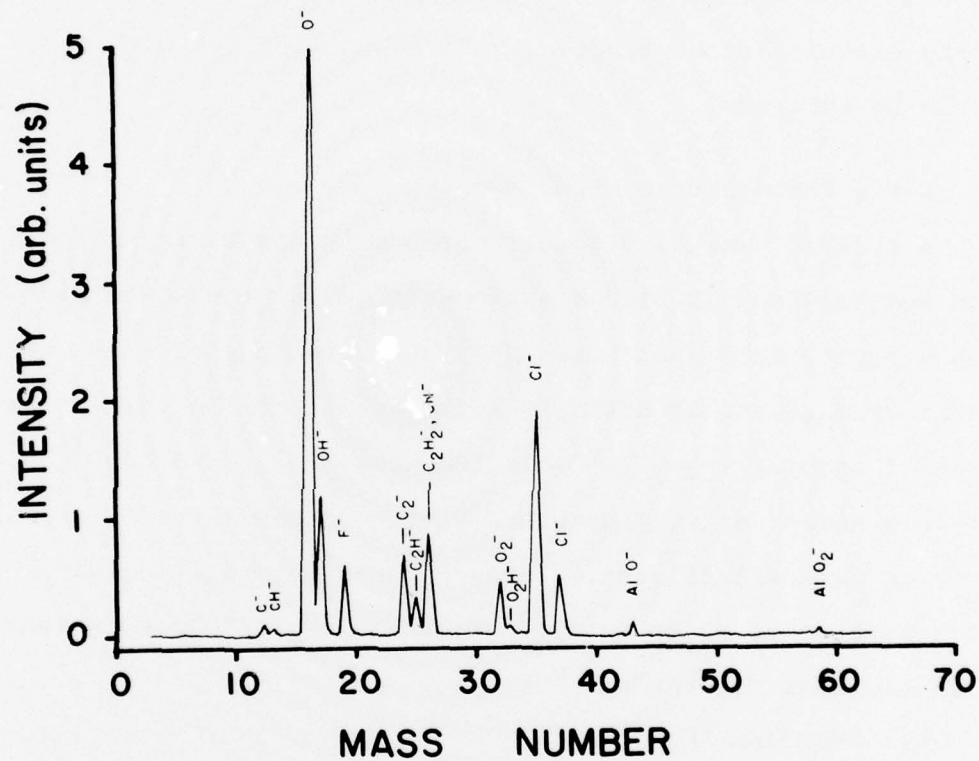


Figure 25 - SIMS spectrum of negative ions emitted by Al surface under argon ion bombardment.

techniques were used to measure the SIMS spectrum. The modulation was applied to a lens in the energy filter. An example of a negative ion SIMS spectrum obtained from an aluminum sample with this system is shown in Figure 25. If a raster and gating circuit is constructed, good depth profiles with SIMS should be obtained.

C. X-ray Photoelectron Spectroscopy

A system¹⁶ was also constructed to enable X-ray Photoelectron spectroscopy (XPS)⁵⁵ measurements to be made under ultrahigh vacuum conditions. One important advantage of this experimental arrangement is that XPS measurements can be made on small areas of samples (<1mm) - "selected area XPS". XPS has been useful in a number of studies where electron beam interactions with surfaces were significant. In fact, XPS was used to monitor the decomposition of CO on metals¹⁵ by measuring the binding energies of the component XPS peaks.

1. Standard XPS spectra

As no handbook of XPS spectra exists a program was begun to build a library of XPS spectra from the elements under medium (4eV) and high (1eV) energy resolutions. Spectra from C, N, O, Mg, Al, Ti, V, Fe, Co, Ni, Cu, Nb, Mo, Rh, Pd, Ag, Sn, Ta, W, Re, Ir, Pt and Au have been documented so far. These data have proven valuable in studying complex systems where the identification of XPS peaks required careful analysis of the data.

2. Comparison with Auger electron spectroscopy

A detailed study was undertaken to compare electron excited Auger signal strengths, X-ray excited Auger signal strengths and XPS signal strengths for a particular system, namely clean nickel and heavily oxidized nickel. It was found that if signal strengths of raw data were used the ratios of signal strengths for corresponding features from nickel oxide and nickel varied widely depending on the particular feature chosen, but if appropriate integrations of the raw data were carried out the ratios obtained were all essentially the same, namely about 0.85. To illustrate this, the results obtained from X-ray excited data are listed in Table 4. Further details of this study can be read in References 16 and 23.

TABLE 4

RATIOS OF CORRESPONDING Ni XPS OR X-RAY EXCITED AES SIGNAL STRENGTHS OBTAINED FROM HEAVILY OXIDIZED Ni TO CLEAN Ni. RATIOS WERE OBTAINED USING PEAK HEIGHTS ABOVE BACKGROUND IN THE RAW DATA AND ALSO USING INTEGRALS OF THE PEAKS. NOTE THAT THE RATIOS OBTAINED FROM PEAK HEIGHTS VARY CONSIDERABLY FROM DIFFERENT AES OR XPS FEATURES, BUT THAT THE RATIOS OBTAINED FROM THE INTEGRALS DO NOT. VALUES OBTAINED FROM TWO EXPERIMENTAL RUNS ARE GIVEN.

<u>AES or XPS feature</u>	<u>Ratio using peak heights</u>	<u>Ratio using integrals</u>
2p _{1/2}	0.39	
	0.44	
2p _{3/2}	0.51	0.82
	0.52	0.85
L ₃ M _{2,3} V	0.76	0.85
	0.81	0.85
L ₃ VV	0.69	0.81
	0.71	0.82
3s	0.7	
	0.7	
3p	0.80	0.88
	0.82	0.88
Valence band	0.76	0.89
	0.81	0.88

SECTION V

DEPTH PROFILE ANALYSES

The techniques developed during the course of this contract have been demonstrated on a number of samples provided by the Air Force. Samples studied include sulfur implanted in GaAs, Zn implanted in CuInSe_2 , Si photodiodes, Be gyro bearing thrust plates, laser impacted Al alloy, detection of Sr in adhesive bonding compounds, and chrome-boehmite filler used for M50 tank bearings.

SECTION VI

CONSTRUCTION AND MAINTENANCE OF EQUIPMENT

During the course of this contract equipment had to be designed and constructed in order to fulfill the requirements of the contract. Some of these items included (a) an electronically timed Ti getter power supply to eliminate electrical noise caused by mechanical clocks, (b) d.c. level shifter delay, 'PLOT' and 'SKIP' circuits for multiplexing, (c) a bake-out control for the ultra-high vacuum system, (d) a 5kV ion bombardment gun power supply, (e) analog integrators, (f) a crystal oscillator for monitoring thin film growth, (g) an interface for a Nicolet signal averager, (h) an automatic filament current control for appearance potential spectroscopy, (i) buffer amplifiers for interfacing, (j) a power supply for high resolution XPS measurements, (k) a collector circuit for an electron multiplier, (l) a scanning sample positioner for sample alignment in XPS, (m) a set of deflectors for ion gun rastering, (n) a set of deflectors for electron beam rastering, (o) an energy filter for SIMS, and (p) components for electron energy analyzers.

The equipment used in the course of the contract was also properly maintained. Items of vital importance included vacuum systems and components, electron and ion guns including filament replacement, and the machining of ceramics to repair electron spectrometers.

SECTION VII

LIST OF PUBLICATIONS

The following papers are based on work carried out under this contract and have been published in scientific journals.

1. "Ion Excited Auger Spectra of Aluminum", Phys. Letters 47A, 317-318 (1974).
2. "Corrections of Auger Electron Signal Strengths for Modulation Amplitude Distortion in a 4-Grid Retarding Potential Energy Analyzer," Surface Sci. 44, 617-623 (1974).
3. "An Easy Method to Accurately Align Ion Bombardment Guns for Depth Profiling in Auger Electron Spectroscopy," Rev. Sci. Instrum. 45, 1113-1114 (1974).
4. "Use of Analog Integration in Dynamic Background Subtraction for Quantitative Auger Electron Spectroscopy - Study of CO on Mo(110)", Surface Sci. 46, 672-675 (1974).
5. "Chemical Effects in the $M_{4,5}$ NN Auger Spectrum of Mo(110) Due to Adsorption of O_2 and CO", J. Vac. Sci. Technol. 12, 325-328 (1975).
6. "Comparison of Auger Spectra of Mg, Al and Si Excited by Low Energy Electron and Low Energy Argon Ion Bombardment", J. Vac. Sci. Technol. 12, 481-484 (1975).
7. Spectrum Subtraction Techniques in Auger Electron Spectroscopy", Surface Sci. 51, 318-322 (1975).
8. "Comparison of Mg $L_{2,3}$ MM Auger Currents Using Electron and Ion Excitation", Phys. Letters 54A, 167 (1975).
9. "Some Factors Affecting Depth Profiling Measurements Using Auger Electron Spectroscopy", Surface Sci. 51, 328-332 (1975).
10. "Appearance Potential Spectroscopy: Relative Signal Strengths from 3d Transition Metals", Surface Sci. 51, 433-440 (1975).

11. "Auger Current Measurements for Quantitative Auger Electron Spectroscopy of Solids", J. Colloid Interface Sci. 55, 370-376 (1976).
12. "Electroluminescence in Br, Cl and Zn Implanted CuInSe₂ p-n Junction Diodes", Appl. Phys. Letters 28, 214-216 (1976).
13. "Some Aspects of an AES and XPS Study of the Adsorption of O₂ on Ni", J. Vac. Sci. Technol. 13, 296-300 (1976).
14. "Oxygen KLL Auger Spectra from O₂ and CO adsorbed on Ni", Solid State Commun. 19, 111-113 (1976).
15. "Auger Electron Spectroscopy Studies of CO on Ni(110) - Spectral Line Shapes and Quantitative Aspects", Surface Sci. 55, 741-746 (1976).
16. "CO-Metal Bond Characterization Using Auger Electron Spectroscopy", J. Electron Spectroscopy 9, 93-97 (1976).
17. "The Application of Tailored Modulation Techniques to Depth Profiling With Auger Electron Spectroscopy", Surface Sci. 60, 1-12 (1976).
18. "Auger Electron Spectroscopy of Solid Surfaces," in "Advances in Characterization of Metal and Polymer Surfaces", ed. L. H. Lee (Academic Press, New York, 1977) pp. 133-154.
19. "The Use of Auger Electron Spectroscopy to Characterize the Adsorption of CO on Transition Metals, Surface Sci. 62, 21-30 (1977).
20. "Zn-Ion Implantation Profiles in CuInSe₂ by Auger Electron Spectroscopy", J. Appl. Phys. 48, 67-72 (1977).
21. "Automatic Correction for Effects of Auger Line Shape Changes on Depth Profiles", J. Vac. Sci. Technol., 14, 232-235 (1977).

SECTION VIII

LIST OF PRESENTATIONS

The following papers based on work carried out under this contract were read at scientific meetings.

1. "Quantification of Auger Electron and Soft X-ray Appearance Potential Spectroscopies Using Integration Techniques", Symposium on Applied Vacuum Science and Technology, Tampa, Florida, February, 1974.
2. "Recent Developments in Quantification of Auger Electron Spectroscopy for Surface Studies", 2nd International Conference on Solid Surfaces, Kyoto, March, 1974.
3. "Auger Spectroscopy Applied to Solid Surfaces", Symposium on the Chemistry of Surfaces, Dayton, Ohio, October 1974 (invited).
4. "Auger Electron Spectroscopy Study of the Adsorption of O_2 , CO and CO_2 on Mo", 21st National Symposium of the American Vacuum Society, Anaheim, October, 1974.
5. "The Production of Auger Electrons by Low Energy Argon Ion Bombardment of Solids", 21st National Symposium of the American Vacuum Society, Anaheim, October, 1974.
6. "Ion Excited Auger Electron Spectroscopy of Solids, Symposium on Applied Vacuum Science and Technology, Tampa, Florida, February, 1975, (invited).
7. "Auger Current Measurements for Quantitative Auger Electron Spectroscopy of Solids", 49th National Colloid Symposium, Potsdam, June, 1975.
8. "Studies of the Adsorption of O_2 and CO on Nickel Using AES and XPS", 22nd National Symposium of the American Vacuum Society, Philadelphia, October, 1975.
9. "Some AES and XPS Studies of the Adsorption of O_2 and CO on Group VIII Metals", 5th Annual Applied Vacuum Science and Technology Symposium, Tampa, February, 1976 (invited).
10. "Auger Electron Spectroscopy of Solid Surfaces", Centennial American Chemical Society Meeting, New York, April, 1976 (invited).

REFERENCES

1. P. W. Palmberg, G. E. Riach, R. E. Weber and N. C. Mac Donald, "Handbook of Auger Electron Spectroscopy", Physical Electronics Industries Inc., Eden Prairie, Minnesota (1976).
2. L. A. Harris, J. Appl. Phys. 39, 1419 (1968).
3. R. E. Weber and W. T. Peria, J. Appl. Phys. 38, 4355 (1967).
4. T. W. Haas, J. T. Grant and G. J. Dooley, J. Appl. Phys. 43, 1853 (1972).
5. H. E. Bishop and J. C. Riviere, J. Appl. Phys. 40, 1740 (1969).
6. N. J. Taylor, Rev. Sci. Instr. 40, 792 (1969).
7. J. E. Houston, Surface Sci. 38, 283 (1973).
8. J. E. Houston and R. L. Park, Rev. Sci. Instr. 43, 1437 (1972).
9. J. T. Grant and T. W. Haas, Surface Sci. 44, 617 (1974).
10. J. T. Grant, M. P. Hooker and T. W. Haas, Surface Sci. 46, 672 (1974).
11. J. T. Grant in "Advances in Characterization of Metal and Polymer Surfaces", Ed. L. H. Lee (Academic Press, New York, 1977) p. 133.
12. D. R. Arnott and D. Haneman, Surface Sci. 45, 128 (1974).
13. G. F. Amelio, Surface Sci. 22, 301 (1970).
14. L. Yin, I. Adler, T. Tsang, M. H. Chen and B. Craseman, Phys. Lett. 46A, 113 (1973).
15. M. P. Hooker and J. T. Grant, Surface Sci. 62, 21(1977).
16. M. P. Hooker, J. T. Grant and T. W. Haas, J. Vac. Sci. Technol. 13, 296 (1976).

11. "Automatic Correction for Effects of Auger Line Shape Changes on Depth Profiles", 23rd National Symposium of the American Vacuum Society, Chicago, September, 1976.

17. T. W. Haas and J. T. Grant, Phys. Lett. 30A, 272 (1969).
18. J. T. Grant and T. W. Haas, Surface Sci. 26, 669 (1971).
19. F. J. Szalkowski and G. A. Somaijai, J. Chem. Phys. 56, 6097 (1972).
20. M. P. Hooker, J. T. Grant and T. W. Haas, J. Vac. Sci. Technol. 12, 325 (1975).
21. M. P. Hooker and J. T. Grant, Surface Sci. 55, 741 (1976).
22. R. W. Springer, T. W. Haas and J. T. Grant, to be presented at the 28th Pittsburgh Conference on Analytical Chemistry and Applied Spectroscopy, Cleveland, Feb./March, 1977.
23. J. T. Grant, M. P. Hooker and T. W. Haas, J. Collid. Interface Sci. 55, 370 (1976).
24. J. T. Grant and T. W. Haas, Surface Sci. 21, 76 (1970).
25. T. W. Haas, J. T. Grant and G. J. Dooley, J. Vac. Sci. Technol. 7, 43 (1970).
26. J. P. Coad and J. C. Riviere, Surface Sci. 25, 609 (1971).
27. J. T. Grant and M. P. Hooker, Solid State Commun. 19, 111 (1976).
28. R. W. Springer, T. W. Haas, J. T. Grant and M. P. Hooker, Rev. Sci. Instr. 45, 1113 (1974).
29. T. W. Haas, R. W. Springer, M. P. Hooker and J. T. Grant, Phys. Lett. 47A, 317 (1974).
30. J. T. Grant, M. P. Hooker, R. W. Springer and T. W. Haas, J. Vac. Sci. Technol. 12, 481 (1975).
31. For a review see: J. D. Garcia, R. J. Fortner, and T. M. Kavanagh, Rev. Mod. Phys. 45, 111 (1973).
32. M. Barat and W. Lichten, Phys. Rev. A6, 211 (1972).
33. J. T. Grant and M. P. Hooker, Phys. Lett. 54A, 167 (1975).
34. J. A. Cairns, A. D. Marwick, and I. V. Mitchell, Thin Solid Films 19, 91 (1973).

35. C. Benazeth, L. Viel and N. Colombie, C. R. Acad. Sc. (Paris) 276B, 863 (1973).
36. J. F. Hennequin and P. Viaris de Lesegno, Surface Sci. 42, 50 (1974).
37. Physical Electronics Industries, model 545.
38. J. W. Coburn and E. Kay, Crit. Rev. Solid State Sci. 4, 561 (1974).
39. K. S. Kim, W. E. Baitinger, J. W. Amy and N. Winogrand, J. Electron Spec. 5, 351 (1974).
40. P. W. Yu, J. T. Grant, Y. S. Park and T. W. Haas, J. Appl. Phys. 48, 67 (1977).
41. Y. E. Strausser and J. S. Johannesson, J. Vac. Sci. Technol. 13, 48 (1976).
42. A. van Oostrom, J. Vac. Sci. Technol. 13, 224 (1976).
43. J. S. Solomon, Appl. Spectroscopy 30, 46 (1976).
44. R. W. Springer and D. J. Pocker Rev. Sci. Instr. 48, 74 (1977).
45. J. T. Grant, T. W. Haas and J. E. Houston, J. Vac. Sci. Technol. 11, 227 (1974).
46. J. T. Grant, M. P. Hooker, R. W. Springer and T. W. Haas, Surface Sci. 60, 1 (1976).
47. J. T. Grant, M. P. Hooker, R. W. Springer and T. W. Haas, J. Vac. Sci. Technol 14, 232 (1977).
48. J. E. Houston and R. L. Park, J. Chem. Phys. 55, 4601 (1971).
49. R. L. Park and J. E. Houston, J. Vac. Sci. Technol. 11 1 (1974).
50. R. L. Park and J. E. Houston, Phys. Rev. B6, 1073 (1972).
51. R. L. Park and J. E. Houston, J. Vac. Sci. Technol. 10, 176(1973).
52. J. E. Houston and R. L. Park, Phys. Rev. B5, 3808 (1972).
53. J. T. Grant, M. P. Hooker and T. W. Haas, Surface Sci. 51, 433 (1975).
54. A. Benninghoven, Surface Sci. 35, 427 (1973).
55. K. Siegbahn et al. "ESCA - Atomic, Molecular and Solid State Structure Studied by Means of Electron Spectroscopy " (North Holland, Amsterdam, 1967).